UPGRADING OF Nd^{3+} LASER AND AIR BREAKDOWN STUDIES

by

D. VICTOR SUVISESHA MUTHU

LASER TECHNOLOGY PROGRAMME

INDIAN INSTITUTE OF TECHNOLOGY KANPUR

JANUARY, 1990

UPGRADING OF Nd^{3+} LASER AND AIR BREAKDOWN STUDIES

A Thesis Submitted
in Partial Fulfilment of the Requirements
for the Degree of

MASTER OF TECHNOLOGY

by

D. VICTOR SUVISESHA MUTHU

to the

LASER TECHNOLOGY PROGRAMME
INDIAN INSTITUTE OF TECHNOLOGY KANPUR

JANUARY, 1990

LTP-1990-M-MUT-UPG

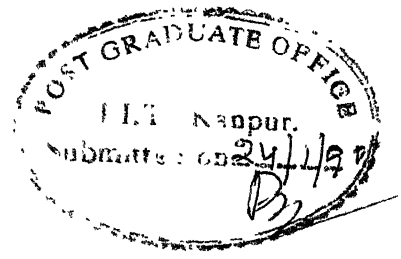

CERTIFICATE

Certified that the work contained in the thesis entitled "Upgrading of Nd^{3+} Laser and Air Breakdown Studies" has been carried out by Mr. D. Victor Suvisesha Muthu under my supervision and the same has not been submitted elsewhere for a degree.

Kanpur

January 24, 1990

(Dr R K THAREJA)

Thesis supervisor

ACKNOWLEDGEMENTS

I am deeply indebted to Dr R K Thareja for introducing me to the subject and for supervising my work with keen interest.

I am very much thankful to Dr Alika Khare for guiding me and helping through out the project.

I would like to thank Dr V Kumar and Ms Rekha Tambay for helping me in my experimental works.

Technical assistance by the staff of the CELT work shop, Mr Kurdeep Singh and Glass blowing workshop is highly acknowledged.

I am very much thankful to Mr M Hajah Mohideen for helping me in preparing the thesis report.

I would like to thank my friends Mansoor, Elango, Tamilselvan, Sampath, Hajah, Immanuel, Lalit, Rajinish, Rangarajan, Dev, Kasi, Uday, Pandimani, Sreeni, Pandian who have made my stay memorable at I.I.T Kanpur.

D. Victor Suvisesha Muthu.

TABLE OF CONTENTS

LIST OF FIGURES

LIST OF TABLES

LIST OF SYMBOLS

E_i - Ionization energy.

λ - Wavelength.

A - Atomic or molecular weight.

τ - Laser pulse duration.

R - Refelctivity of metal surface.

h - Plancks constant.

ν, ω - Frequency.

E_p - Photon energy.

I - Incident laser intensity.

P - Pressure.

θ - Polarization angle.

B - Magnetic field strength.

V - Verdet constant.

η - Refractive index.

μ_o - Permeability of air.

N - Total no. of turns.

r - Effective radius of solenoid

i - Current through the solenoid.

j - Overall current density.

f - Focal length of lens.

LIST OF SYMBOLS

E_i - Ionization energy.

λ - Wavelength.

A - Atomic or molecular weight.

τ - Laser pulse duration.

R - Refelctivity of metal surface.

h - Plancks constant.

ν, ω - Frequency.

E_p - Photon energy.

I - Incident laser intensity.

P - Pressure.

θ - Polarization angle.

B - Magnetic field strength.

V - Verdet constant.

η - Refractive index.

μ_o - Permeability of air.

N - Total no. of turns.

r - Effective radius of solenoid

i - Current through the solenoid.

j - Overall current density.

f - Focal length of lens.

Name of the student: D. Victor Suvisesha Muthu. Roll No.: 8811602

Department: Laser Technology Programme

Title of the Thesis: Upgrading of Nd^{3+} Laser and Air Breakdown Studies.

Name of the thesis supervisor: Dr R K Thareja

ABSTRACT

An existing Nd:Glass laser was upgraded and obtained energy as much as 80J per pulse. Air breakdown studies using Nd:Glass and Nd:YAG lasers were performed. Effect of metal plasma was studied to breakdown air using Nd:Glass laser. The wavelength dependence and pressure dependence of air breakdown threshold were studied using the Nd:YAG laser and its harmonics. Dependence of the size of visual spark as a function of laser radiation was studied. To avoid the back reflection from the laser produced plasma, a Faraday isolator was designed and the performance charateristics of various components of the isolator are presented.

CHAPTER 1

INTRODUCTION

Since the first reports by Maker et al[1] and Mayerand et al[2] on gas breakdown at optical frequencies by means of a Q-switched laser, there have been many reports on optical breakdown of gaseous medium by Agostini et al[3] and Grey Morgan[4].The phenomenon is observable at very high field strength ($>10^6$V/cm for atmospheric gases), which can easily be obtained by focussing a high power laser beam. Laser field as strong as coulomb field applied to an atom removes the valence electron away from an atom and the gas breakdown is observed. For example,in the case of atmospheric air the breakdown is characterized by a flash of bluish white light at the focus accompanied by a distinctive cracking noise. In the case of solids breakdown is defined by a damage spot. Laser induced gaseous and metal plasmas have several applications in various fields of research. Laser triggered spark gaps[5] have been developed and extensively used in highvoltage switches. Laser induced rare gas plasmas are found as a source of VUV radiation. Laser induced metal plasmas have been used as a source of high intensity X-rays, and for photoionization lasers. If the plasma density is very high plasma mirror effect[6] is observed and which acts as an optical Q-switch.

The laser interaction studies have usually been done using Nd:YAG or Nd:Glass or CO_2 lasers. Since CO_2 lasers require special optics etc for working, an extensive work has been reported using Nd^{3+} lasers. We have upgraded an existing Nd:Glass laser and used for studies air breakdown near a metallic surface. The details of the changes made are described in chapter 2. Due to nonavailability of index matching fluid for Pockel's cell the use of laser was limited to free running mode ie, non Q-switched operation. The laser delivered as much as 80J per shot. On focussing laser irradiation on to a solid target it was possible to see characteristic plasma of the target used. In such cases it is possible that a part (5%to25%) of incident radiation may be reflected back by the plasma. To avoid the possibility of this back reflected radiation going back in to oscillator an optical Faraday isolator was designed. The reflected radiation reaching the oscillator, in the absence of an isolator, may damage optical components in the way and even the laser rod. The details of the design and performance characteristics of Faraday isolator are presented in chapter 3.

There have been reports on the observation of breakdown of the gases with low power lasers in the presence of preionization. The initiatory electron can be provided by either applying static electric field transverse to the laser focus, or due to presence

of low ionization potential gas or by metal surfaces.Smith[7] has shown that preionization densities $\approx 10^{11}cm^{-3}$ lowers the threshold. Robinson[8] reported similar results for preionization densities as low as $10^{10}cm^{-3}$. Decrease in threshold energy of breakdown of atomic and molecular gases in the presence of metallic surface using a CO_2 laser has also been observed Vedenov et al[9] have shown theoretically that breakdown of a gas is due to thermal ionoztion of metal vapor of low ionization potential. The minimum intensity, $I(W/cm^2)$, required for the development of an electron cascade in the gas is given by[10]

$$I>6\times10^{9}Ei/\lambda^{2}A$$

where Ei is the first ionization energy (ev) of the gas, λ is the wavelength (μm) of laser radiation and A the atomic or molecular weight of the gas.Barchukov et al reported that a spherical shock wave (point explosion) develops in a small region of dense vapour near the target with in a time $t=d/u \ll \tau$ (the laser pulse duration), where d is the laser radiation spot size on the surface of target and u the speed of sound in the vapour. The threshold intensity of the developed evaporation regime of the metallic and non-metallic surface can be determined by the estimates $I^{m}_{evp} \geq 10^{7}/(1-R)$ W/cm^2 where R is the reflectivity of the metallic surface at $1.06\mu m$ and $I^{nm}_{eva} \leq 10^{6}(1-R)$ W/cm^2. We have studied the effect of metallic surface on the breakdown of

air using a free running Nd^{3+} laser. It is the first report, author's claim, that such studies are reported. chapter 4 describes the experimental observations.

Laser Induced Gas Breakdown

In the field of an intense laser beam electrons may be generated in a gas by two mechanisms[11] direct multiphoton ionization (MPI) and electron impact or cascade ionization. In the first process, an atom or molecule of ionization energy E_i absorbs n simultaneous photons of energy $h\nu$, subject to the condition $nh\nu \geq E_i$, and thereby becomes photoionized, where $n=(E_i/E_p)$ where E_p is the photon energy. The ionization rate varies as I^n and the electron density, for a constant intensity pulse, increases linearly with time. Multiphoton ionization is dominant when the laser beam of intensity $\geq 10^{11} W/cm^2$, at low gas pressure $\leq 10^{-3}$ torr, at wavelength below 1μm and when $pt \leq 10^{-7}$ torr-sec. The pressure dependence of MPI process is very weak and it varies as $p^{-1/n}$. Bebb and Gold[12] concluded that although MPI may provide the initial electron, it doesnot account entirely for the breakdown phenomenon except possibly at very low pressure. In the second process, electrons gain energy from the laser field through inverse bremsstrahlung (IB) collisions with neutrals. The electrons can readily ionize the gas when their energy exceeds

E_I. At sufficently high fields, ionizing collisions will cause an electron cascade to occur with the electron density increasing exponentially with time. Cascade ionization process is dominating when the gas pressure $\geq 10^2$ torr, when the wavelength $>1\mu m$ and when $p\tau \geq 10^{-7}$ torr-sec. The pressure dependence of threshold in the case of cascade ionization process varies as p^{-1}. We have used DCR4 (Spectra Physics) Nd:YAG laser and its harmonics to study breakdown of air at various pressures. In Chapter 5 we report the dependence of threshold energy required to breakdown air using 1.06, 0.55, 0.355, 0.266μm irradiation at various pressures. Preliminary results on the dependence of size of breakdown region on pressure, wavelength and threshold energy are presented.

CHAPTER 2

EXPERIMENTAL TECHNIQUE

In this chapter we briefly discuss the development workdone to upgrade the existing Nd^{3+} laser system and the design of target chamber. The Nd:Glass laser used in our studies is a Holobeam 800 series pulsed system. In this laser an optical glass rod is doped with Nd^{3+} ions. Normally about 1% to 3% [13] of Nd^{3+} ions are doped in the glass. The pump bands of Nd^{3+} ions are shown in the energy level diagram (figure2.1). The laser transition at 1.06μm corresponds to transition $^4F_{3/2}$ to $^4I_{11/2}$.

This Nd:Glass system contains

i) Laser head and heat exchanger

ii) Laser power supply and remote station

iii) Pockels cell assembly

The laser head contains a Nd:Glass rod of length 20.3cm and diameter 1.9cm. The rod is optically pumped by a helical, Xenon-filled arc discharge flashlamp. The radiation from the flashlamp is coupled into the rod by direct radiation from the flashlamp and through the reflected radiation from the reflector. The whole assembly, laser rod and flashlamp is filled with recirculated deionised water. The laser resonator consists of two dielectric coated mirrors, rear mirror with maximum reflectivity at 1.06μm and output mirror with 18% reflectivity. Cold water

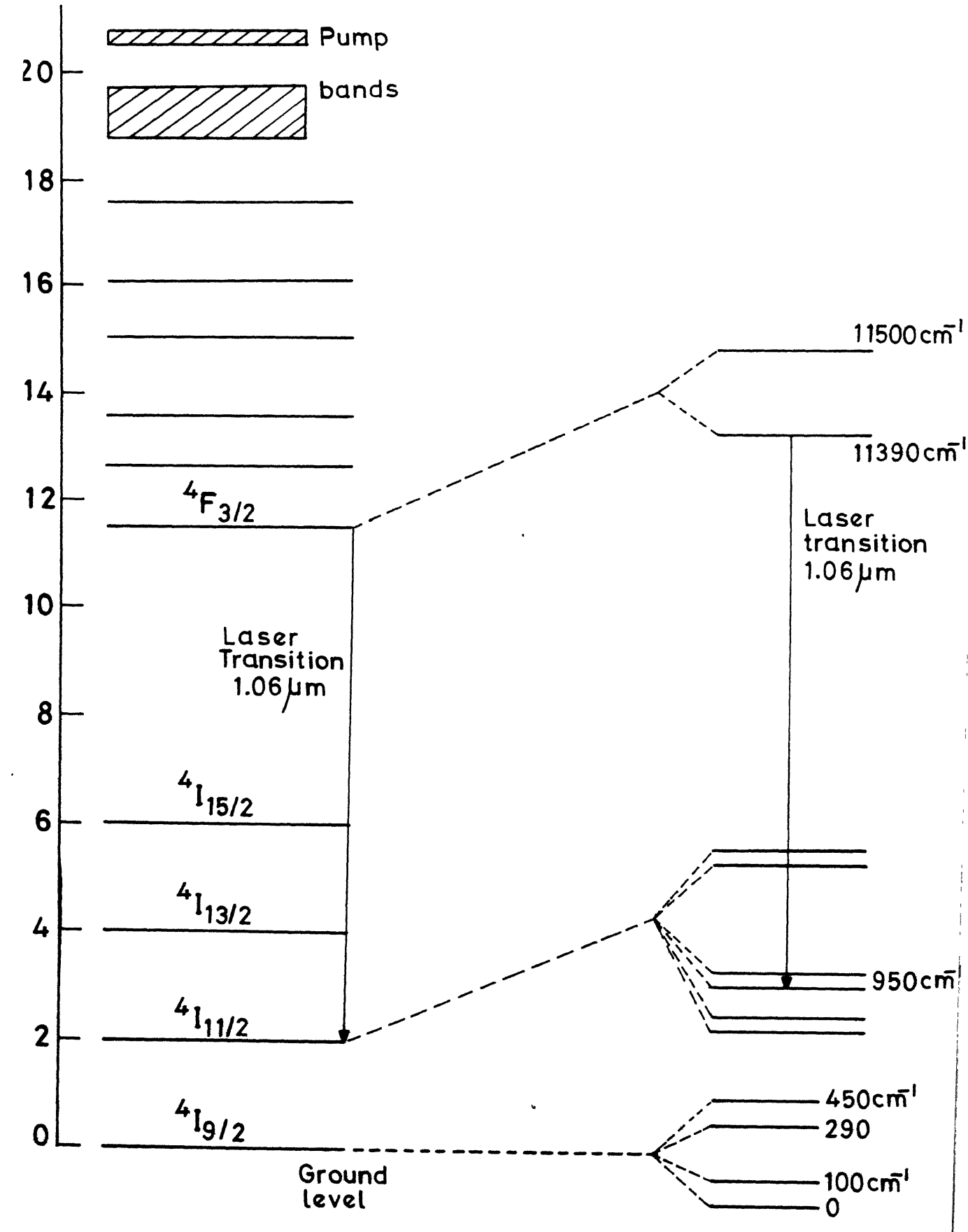

Energy Level Diagram of Nd^{3+} in glass

is circulated through the laser head by using a heat exchanger It contains a cooler and a water recirculating system. The heat exchanger is designed in such a way that the whole laser head is kept at a temperature of 23°C continuously through out the operation of the laser. Since the cooler in the heat exchanger was not working, a closed cycle recirculating water system arrangement was designed using a small external cooler.

The power supply is operated by 220 volts 60 Hz ac source It contains a PFN capacitor bank in which energy is stored first and later discharged in the flashlamp. The PFN capacitor bank is charged by the transformer supply voltage through the SCRs. This part of this circuit was not working, charging circuit were changed using equivalent SCRs etc. The energy storage and release are done by the power supply remote station upon command from the charging circuit and firing circuit.

The Pockels cell assembly contains KDP crystal in an index matching fluid cell, a polarizer and the rear mirror.During the flashlamp fire the Pockels cell is closed and after a delay time, on the application of a high voltage the Pockels cell opens and lasing occurs in a giant pulse. Initially Q-switched mode operation was tried but it was found out there was no index matching liquid inside the Pockels cell. Without this liquid it is not safe to operate Pockels cell. So the laser was operated in

the free running mode only.

The free running mode configuration is shown in the figure 2.2, and the charging electrical configuration is shown in figure 2.3. The laser was aligned using a He-Ne laser by coinciding the reflected beams from the two mirrors with the direct beam. The output energy was monitered by an energy meter(scientech) put in the path of the beam. A curve of input supply voltage to the flash lamp and the optimum output laser energy was plotted for future reference. This is shown in the figure 2.4. The pulse shape of the laser output was also observed using an oscilloscope was found to be about 1-2msec. It was not possible to resolve various peaks in the profile with the oscilloscope used. To avoid the possibility of laser radiationback reflected from laser produced plasma entering into the laser cavity, a Faraday isolator for use after the laser oscillator was designed (chapter 3).

Target chamber and Vacuum system

The target chamber used in the studies is made of MS,the inside of which is chrome coated. It has three window as shown in figure 2.5. A metallic target can be introduced from top and could be rotated in vacuum with the help of an external motor at a desired speed. On all the three windows quartz, blanks were used. One of the three windows was used for laser input which was

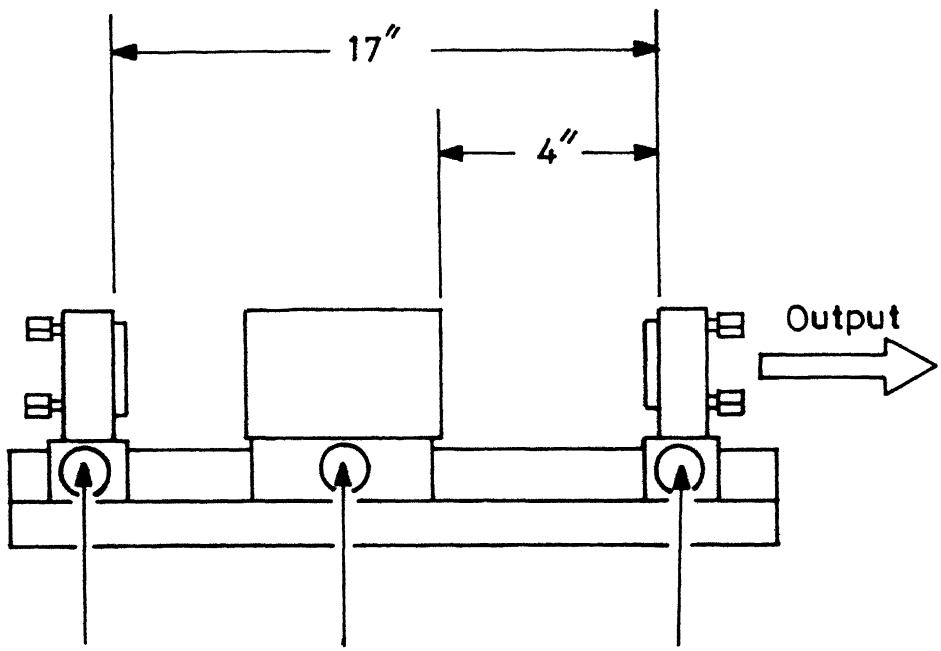

Component Configuration or Conventional Mode Operation.

FIG. 2·2

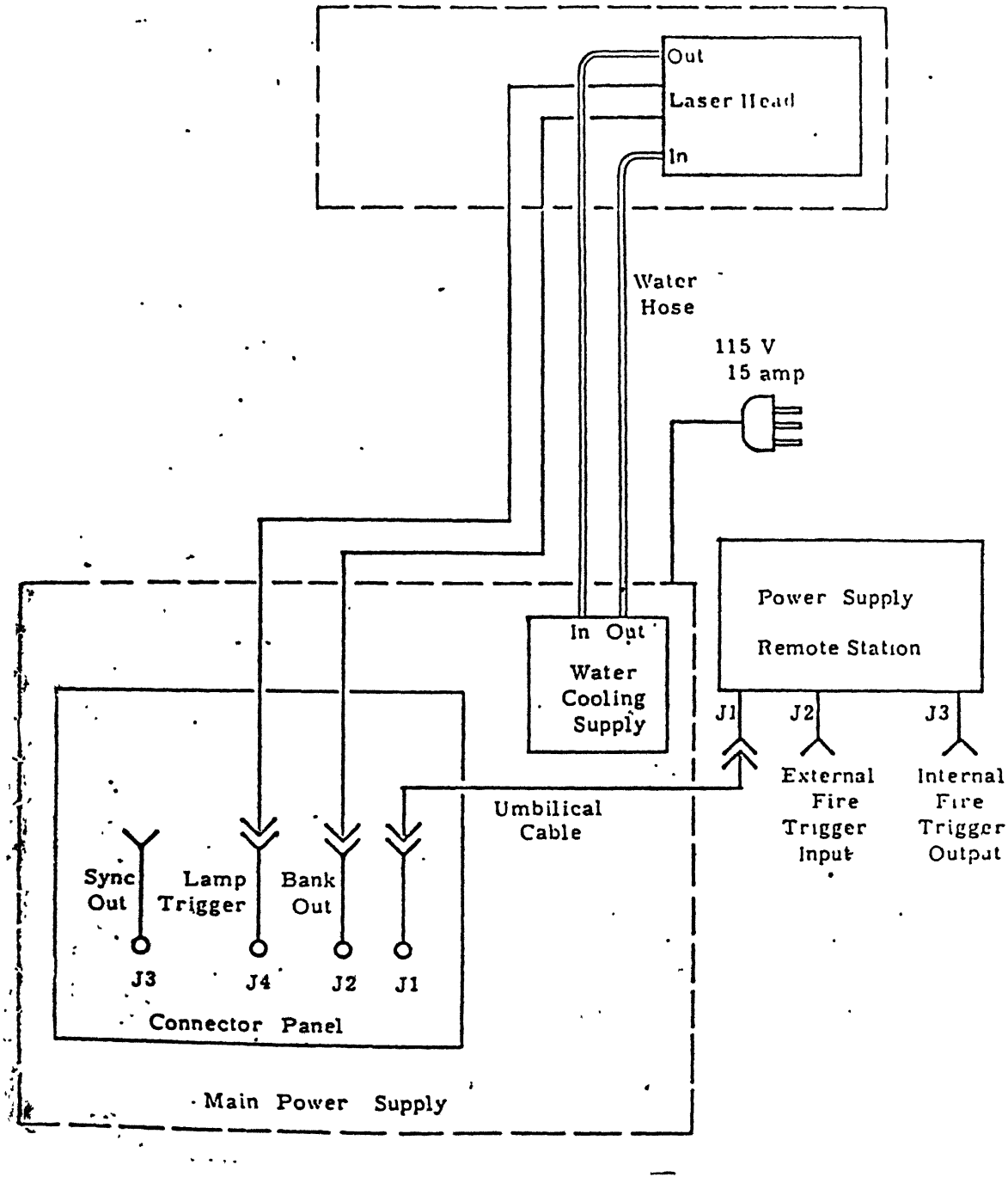

FIGURE 2-3a

Pulsed Laser System - Interconnection Diagram for Conventional Mode Operation

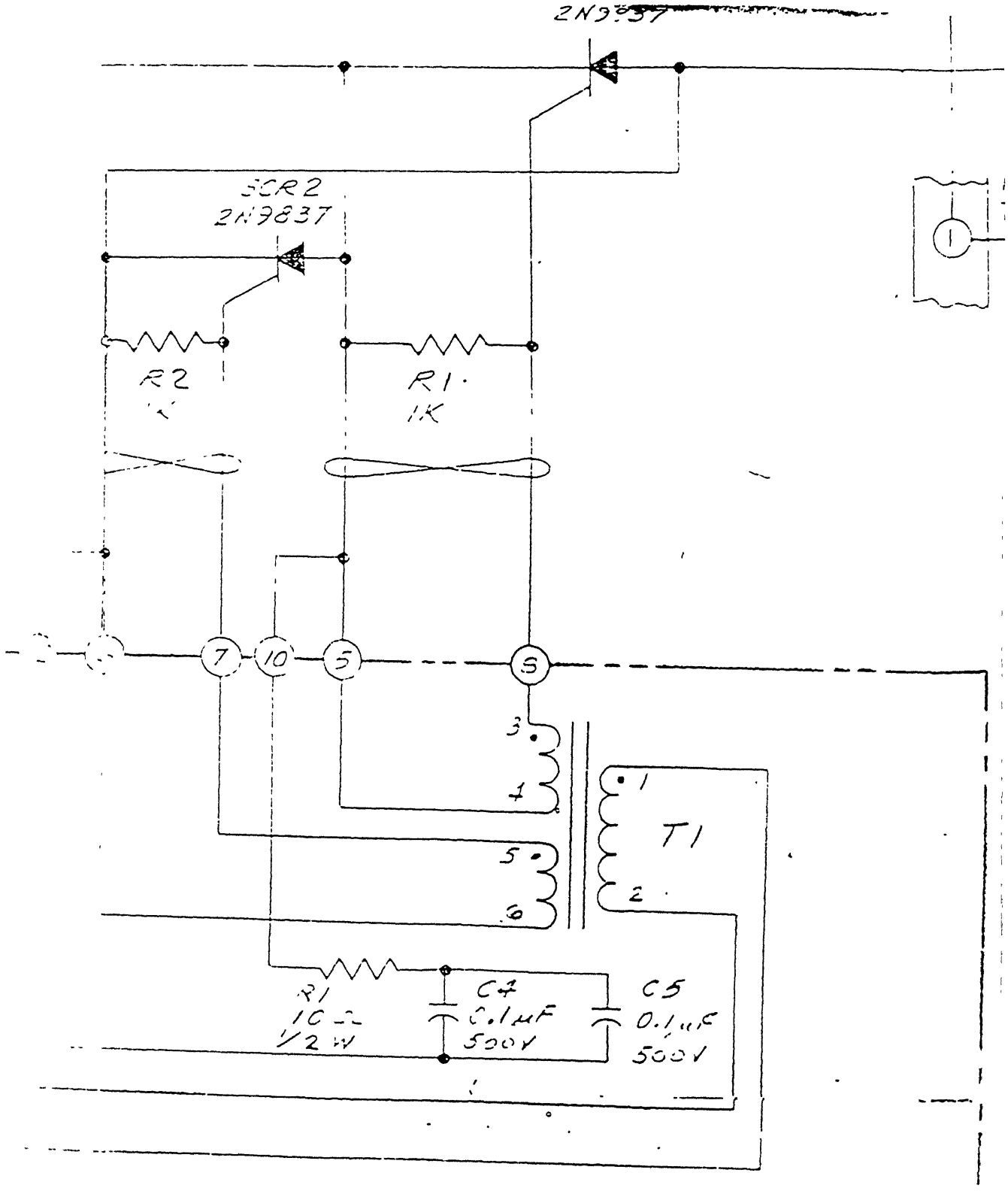
2N3837
SCR2
2N3837
R2
1K
R1
1K
7
10
5
S
3
4
1
T1
5
6
2
R1
10Ω
1/2 W
C4
0.1μF
500V
C5
0.1μF
500V

FIG 2-3b

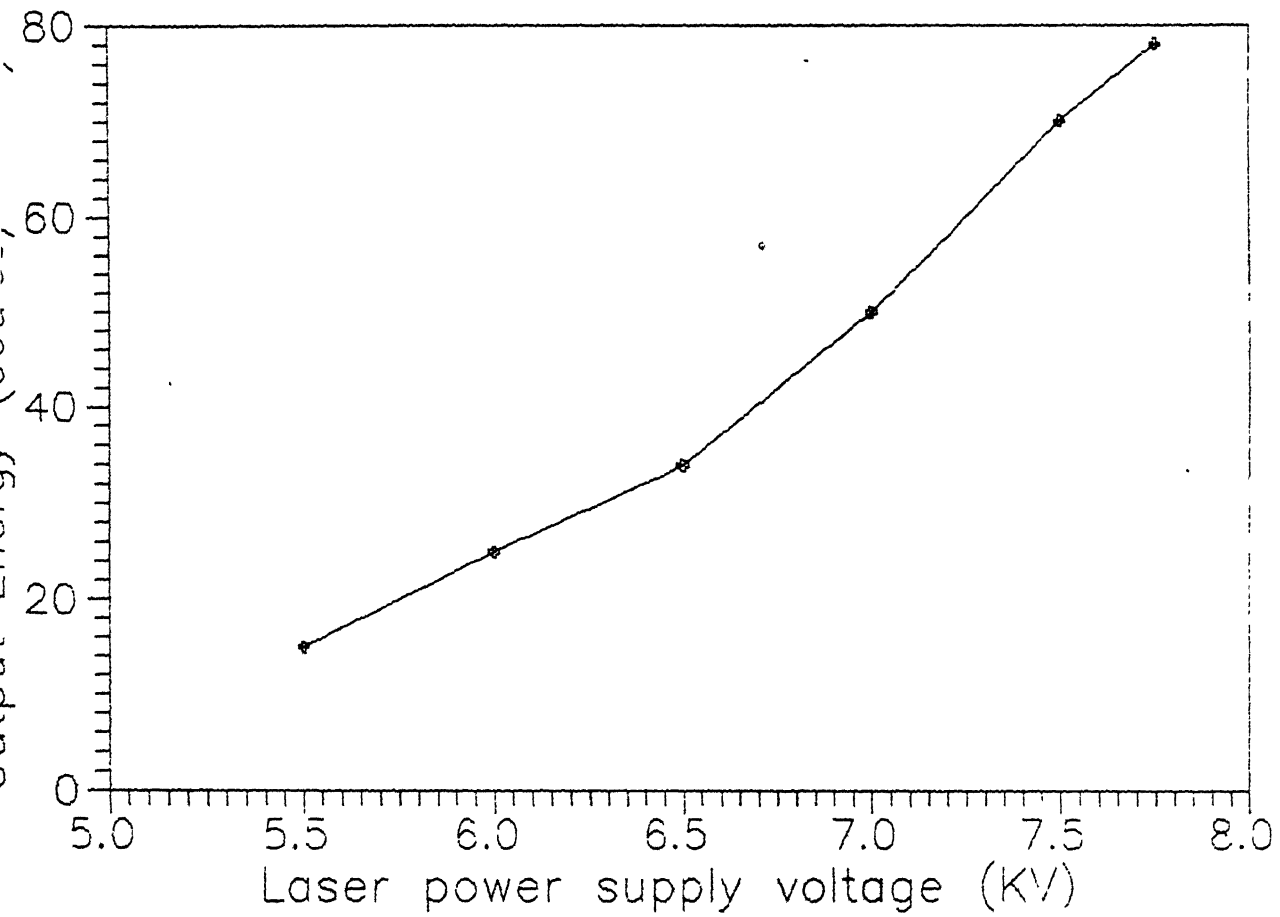

Fig. 2·4 Voltage Vs Output Energy

focussed on to the target with a lens placed outside the chamber. Out of the other two windows, one was used for recording spectrum and the other for viewing the plasma and taking photographs of the plasma. Target chamber was evacuated to a pressure of better than 10^{-4}torr using a rotary pump and an oil diffusion pump. In order to have specific pressure in the target chamber, it was separated from the vacuum system by an extra valve. A thermocouple gauge, a penning gauge and an oil monometer were attached to monitor the pressure after the rotary pump, and pressure inside the chamber respectively. The complete layout of target chamber along with vacuum system is shown in figure 2.6.

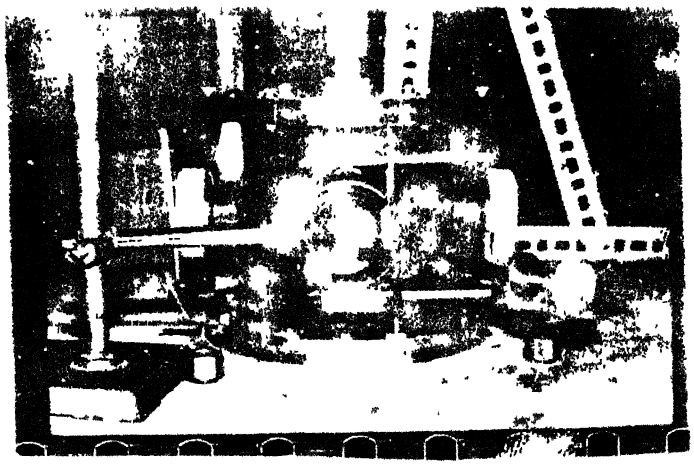

FIG. 2·5 Target Chamber

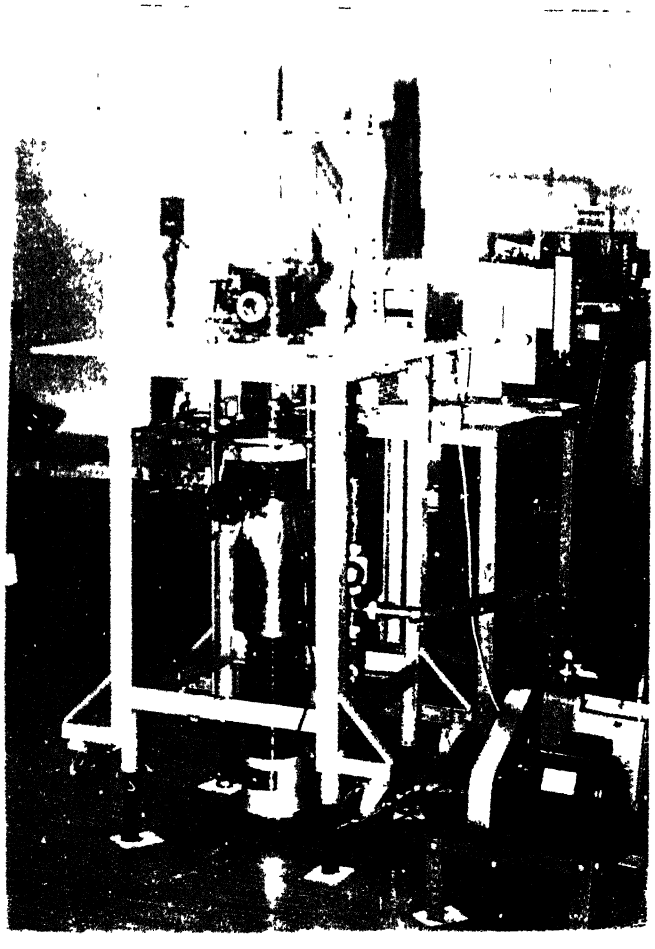

FIG 2·6 Target Chamber with Vacuum system

CHAPTER 3

FARADAY ISOLATOR FOR HIGHPOWER Nd:GLASS LASER

Introduction

When high power laser is focussed flux densities of the order of 10^{14} Watt/cm^2 can be achieved. Ifsuch a high power laser radiation is focussed on to a solid target to produce plasma, a considerable amount (5% to 25%) is reflected by the plasma back through the laser amplifier configuration. If this reflected radiation is not suppressed completely then amplification of reflected light causes damage to the optical components of the laser. Hence experiments with high-power laser amplifier configurations often need, an isolator. Isolator suppresses self-oscillation of the configuration and also acts as an effective protection against laser radiation being reflected back into the amplifier configuration. Although several possible methods are available but an optical isolator based on the Faraday Effect seems to be the best choice for suppressing the back reflected radiation. In this chapter we discuss the principle of a Faraday Isolator, design consideration and its performance.

Operating Principle

If a plane polarized light passes through a material kept in a magnetic field with the direction of magnetic field parallel to that of propagation, the plane of polarization of the incident light is rotated. This effect iscalled Faraday effect[14]. The change in polarization angle θ is given by θ=VBL , where L is the length of Faraday active material, B is the magnetic field strength and V the verdet constant of the material. The principle of Faraday isolator[15] can be understood with reference to Figure 3.1 . The laser beam coming from the laserhead, may be anoscillater as in our case or a chain of amplifier, first passes through the polarizer P_1. The light then passes through a glass rod kept in a magnetic field. The magnetic field is chosen in such way that the plane of polarization of the beam emerging from the glass rod is rotated by 45°. This light passes through the polarizer P_2kept at an angle of 45° with respect to polarizer P_1. If radiation is reflected back through the polarizer P_2 and passes through the glass rod it is further rotated through 45°. The polarizer P_1 is thus in the blocking direction with respect to the reflected light. A plane polarized light can be considered as a linear sum of right circularly and left circularly polarized components, if this light passes through a medium of length l placed in a magnetic field the phase difference between the two

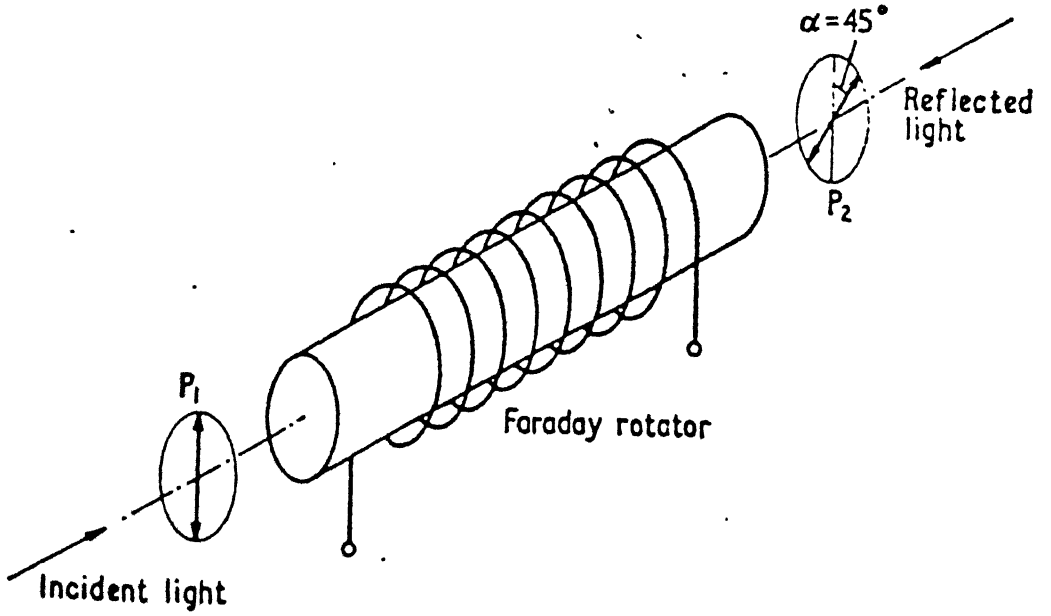

Principle of the optical isolator

FIG. 3.1

components is $\phi=2\pi/\lambda\ (\eta_- - \eta_+)l$. If the refractive index η_+ is smaller than η_- right circular component will move with greater velocity and rotated in the positive direction. The amount of rotation depends on the length of the medium and the strength of the magnetic field. If η_- is smaller than η_+ the rotation will be in the negative direction.

Design of Faraday isolator

Glass for Faraday rotators

The Faraday material used should meet the following requirements

i) high verdet constant

ii) low absorption at the laser wavelength ie., 1.06μm

iii) high damage threshold

iv) very low strain induced birefringence and refractive index variation.

Table 1 gives the verdet constant of the glass usually used in an isolator

Glass	Verdet constant(min/oer/cm)
M-16	0.077+0.0003
ED-4	-0.0061.7
SF-6	+0.0281.85
FR-5	-0.0712.0
FR-4	-0.0311.72

Out of these glasses M-16 seems to be the best choice for the isolator, it has a high verdet constant and low absorption at 1.06μm A rod of length 5cm diameter 2cm was chosen in our design.

Design of polarizers

Two polarizer as shown in Fig.3.1 are required for the Faraday isolator. Since the aperture of the laser is more than 1.5cm and output energy is very high, the usual calcite polarizers become very expensive and difficult to obtain. Considering these factors stacked-plate polarizers (pile of polarizer) were made with high polarizance and low absorption at the laser wavelength. Advantage of these polarizers are, they can be made with any desired aperture and damaged plates can be replaced easily.

For m plates of refractive index n, mounted at Brewster's angle the degree of polarization produced by the polarizer is given by[16]

$$P = \frac{1-(2n/(n^2+1))^{4m}}{1+(2n/(n^2+1))^{4m}}$$

The polarizance was calculated using the above relation and the transmission was calculated using the relation $T = 100(1-4/100)^m$. Figure 3.2 shows the variation of degree of polarization and transmission intensity with number of glass plates. It clearly shows that for lower number of plates the degree of polarization

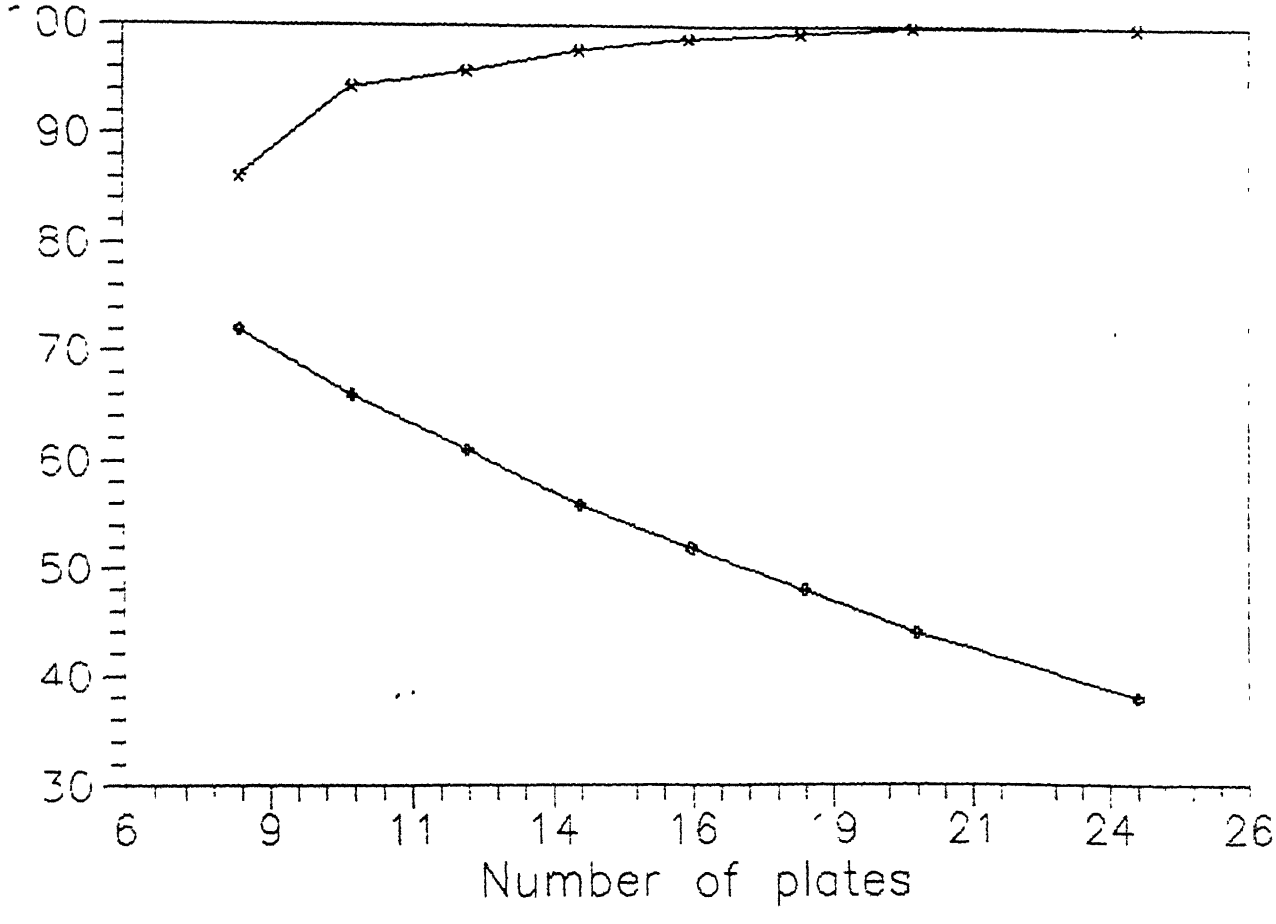

Fig.3-2 Number of plates Vs Transmission & Polatization

is low and the transmittance is high, and for higher number of plates the degree of polarization is high but the transmittance is poor. The polarizer was made for 8 plates for which the degree of polarization is 86% and the transmission is 72% .Due to nonavailability of 2mm thick glass plate, two glass plates of thickness .8mm were mounted in a sigle groove.

We used glass plates of 0.8mm thick, length 3.7cm, and width 2.3cm mounted at Brewster's angle. A lay out of plates is shown in the figure 3.3. This mount was fixed inside a hollow aluminium tube of outer diameter 5.6cm and length 5cm. The entire assembly was fixed inside another hollow cylinder of 3 cm outer diameter. The cylinder containing the pile of polarizer mount can be rotated through 360° and the angle of rotation can be directly read on the dial.

Performance of the polarizer

The transmission intensity of the polarizer was measured by rotating one polarizer through 360° with respect to the other polarizer in steps of 10°. The light beam from a He-Ne laser passes through the two polarizers and falls on a photodiode. The photodiode output was fed to a CRO. The signal was plotted. figure 3.4, against angle of polarization which shows maximum transmission at the parallel position and the minimum transmission at the perpendicular position. The measured

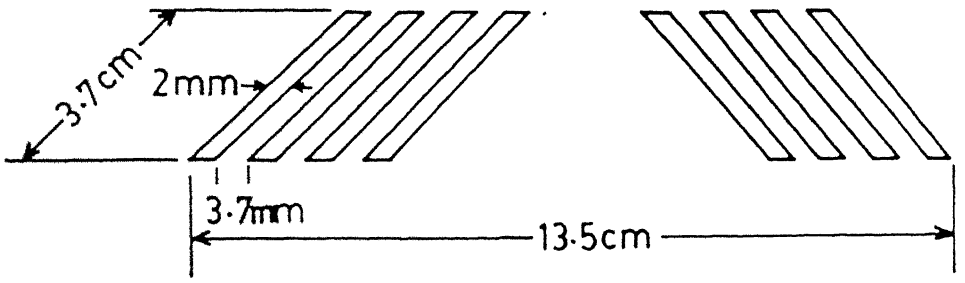

FIG. 3-3 SKETCH OF 8-PLATE PILE OF POLARIZER

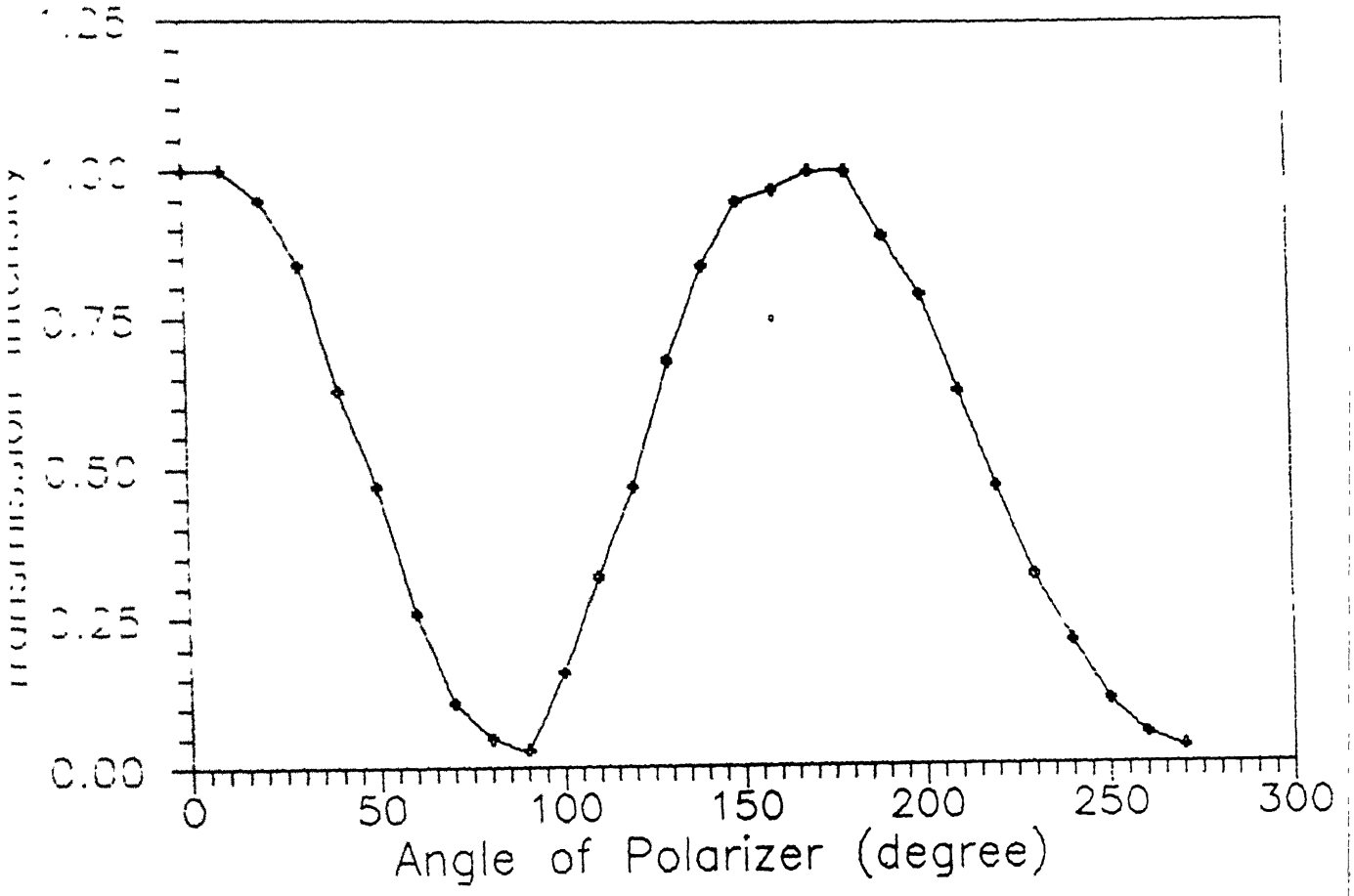

Fig. 3-4 Transmission Intensity of pile of polarizer at different angle

transmittance at the parallel position was 43% and the minimum 1.3% . Passive extinction ratio of the polarizers was measured to be 34dB.

Magnetic field generation

For a glass rod (M16) of length 5cm with verdet constant 0.077 min/oer-cm , to get 45° rotation of polarization requires a magnetic field of 7 KG. This magnetic field was obtained using pulsed air-core solenoid. It has an additional advantage that it does not require any elaborate cooling system, and the rotator can be made compact.

Design consideration

Figure 3.5 shows an air-core solenoid of length 13.5cm and diameter 4cm tightly wound with copper wire in a single layer of 120 turns. At any point along the longitudinal axis the magnetic field strength is approximately[17] given by

$$B(x) = \mu_o Ni/2l \{(l-x)/[r^2+(l-x)^2]^{1/2}+x/(r^2+x^2)^{1/2}\} \quad \ldots(1)$$

where μ_o is the permeability of air ($4\pi \times 10^{-7}$ H/m), Nthe is total number of turns, l is the length of the solenoid, i is the current through the solenoid, and r the effective radius of the solenoid. B(x) is maximum at the center of the solenoid and for this point

$$B_{max}(x=1/2) = \frac{\mu_o Ni}{(4r^2 + l^2)^{1/2}} \quad \ldots(2)$$

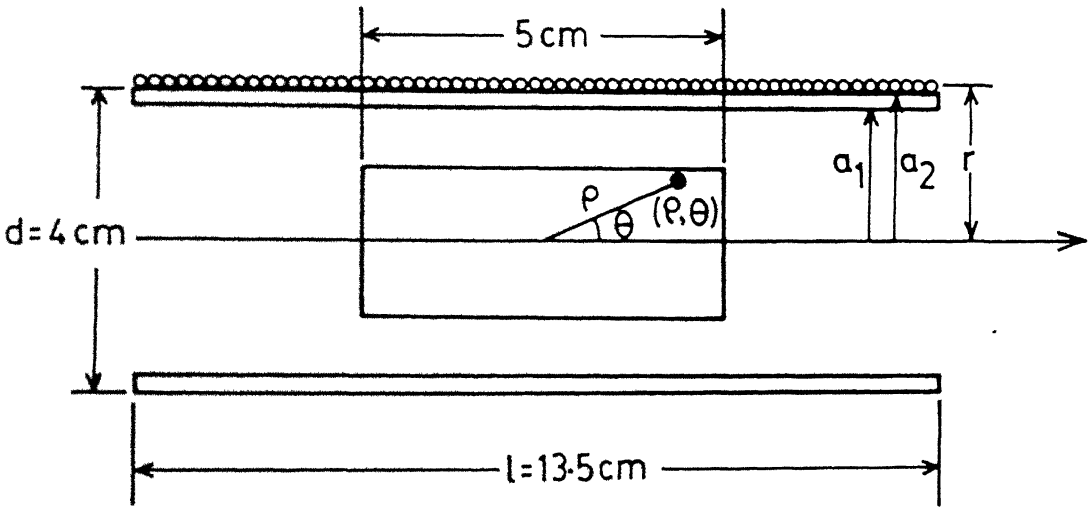

ss section of air-core solenoid [120 turns of copper wire]

Effective radius of solenoid - 2·05 cm

a_1 - 1·8 cm a_2 - 2 cm

ss rod length - 5 cm Diameter - 2 cm.

G. 3·6

To account for the decrease in field strength toward the end of the coil, define a flux linkage factor k as the ratio of the average field strength to the maximum field strength.

$$k = \frac{B_{ave}}{B_{max}} = [4(r/l)^2+1]^{1/2}\,\{[(r/l)^2+1]^{1/2}-r/l\} \qquad \ldots\ldots(3)$$

For various ratios of coil length to radius the flux linkage factor k is calculated and is plotted in figure 3.6. From the graph, a ratio of coil length to radius is taken 6.75 and the corresponding k value is 0.898.

Since the field strength falls gradually away from the center the glass rod is placed at the center of the long solenoid as in figure 3.5. The axial variation of the field using equation (1) was calculated for various points along the field axis and is plotted in figure 3.7. From the plot one can see the variation inside the glass rod is very low.. If there is a small variation in the field then the backward transmission can be written as[18]

$$T = \pi^2/16\,(\Delta H/H)^2. \qquad \ldots\ldots(4)$$

The axial magnetic field at any point inside the solenoid is given by[19]

$$H_z(\rho,\theta) = j\,a_1\,\{F(\alpha,\beta)+F(\alpha,\beta)E_2(\rho/a_1)^2P_2(u)+F(\alpha,\beta)E_4(\rho/a_1)^4 P_4(u)+.....\} \qquad \ldots\ldots(5)$$

where j defines the overall current density

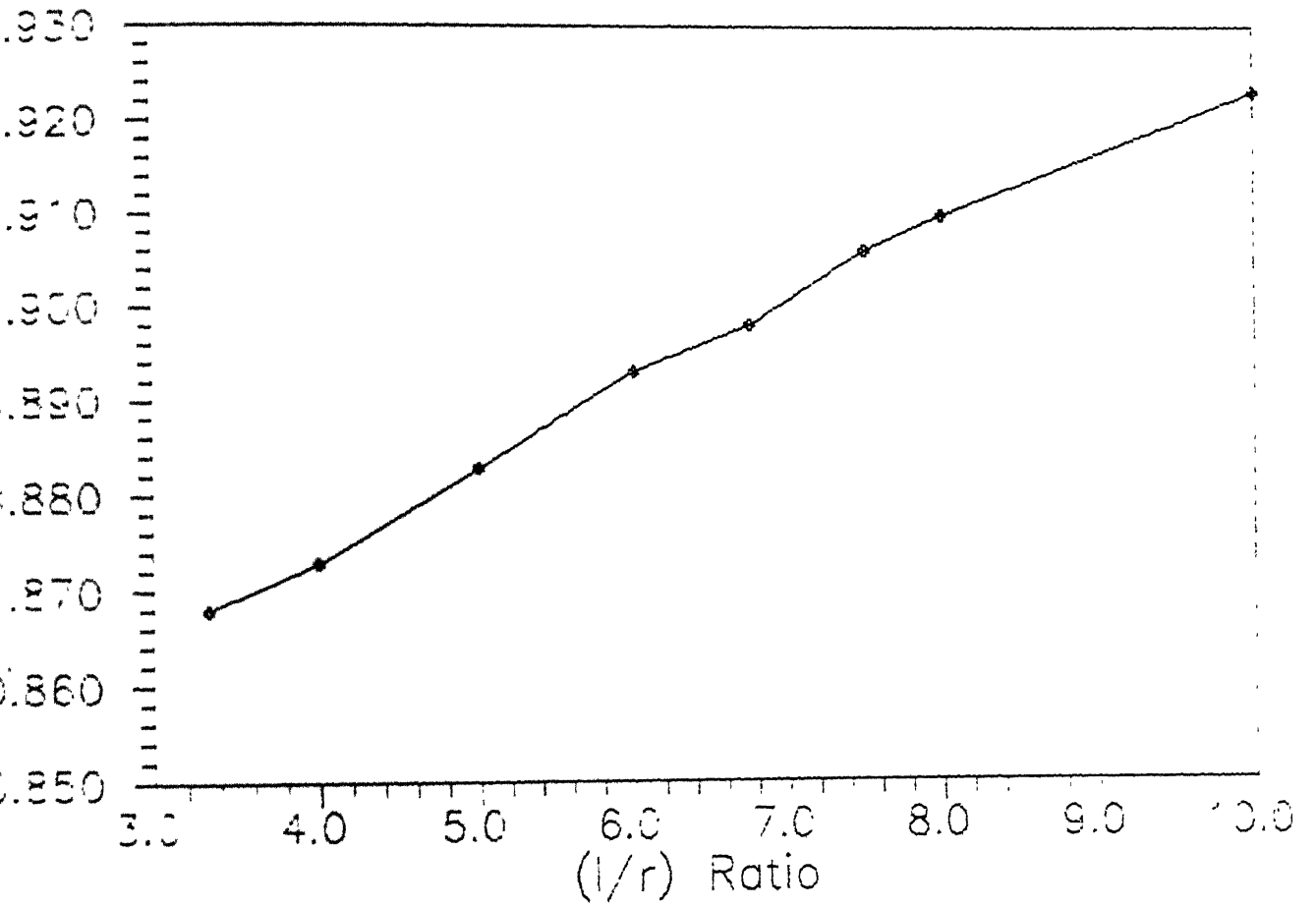

Fig.36 Flux linkage factor Vs (l/r) Ratio

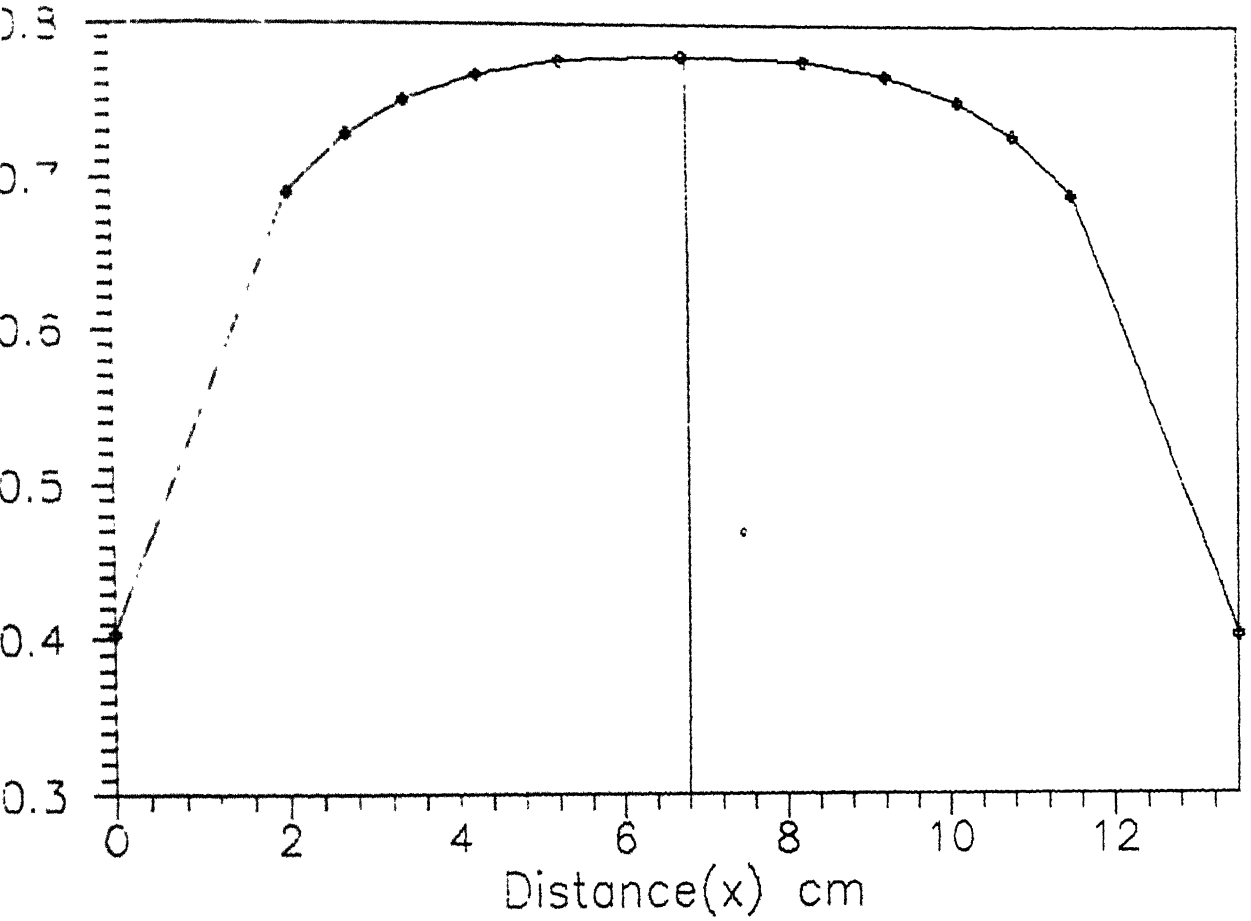

Fig. 3-7 Axial variation of Magnetic field strength inside the solenoid

$$B = \frac{NI}{2b(a_2 - a_1)} \cdot 2b=1$$

$F(\alpha,\beta)$ is defined as the 'field factor' and

$$F(\alpha,\beta) = 4\pi\beta/10\ (\sinh^{-1}\alpha/\beta - \sinh^{-1}1/\beta)$$

or

$$F(\alpha,\beta) = 4\pi\beta/10\ \ln\frac{\alpha+(\alpha^2+\beta^2)^{1/2}}{1+(1+\beta^2)^{1/2}}$$

with $\alpha = a_2/a_1$ and $\beta = 1/2a_1$

First few the Even-Order Legendre polynomials and Error coefficients are given below

$P_0(u) = 1 \qquad u=\cos\theta$

$P_2(u) = 1/2\ (3u^2-1)$

$P_4(u) = 1/8\ (35u^4-30u^2+3)$

$P_6(u) = 1/16\ (231u^6-315u^4+105u^2-5)$

$F(\alpha,\beta) = 4\pi\beta/10\ (\sinh^{-1}\alpha/\beta-\sinh^{-1}1/\beta)$;

$F\ E_2(\alpha,\beta) = 4\pi/10*1/2\beta\ (C_1^{3/2}-C_3^{3/2})$

$F\ E_4(\alpha,\beta) = 4\pi/10 * 1/24\beta^3[C_1^{3/2}(2+3C_2+15C_2^2)-C_3^{3/2}(2+3C_4+15C_4^2)]$

where

$C_1=1/1+\beta^2$; $C_2=\beta^2/1+\beta^2$; $C_3=\alpha^2/\alpha^2+\beta^2$; $C_4=\beta^2/\alpha^2+\beta^2$

The magnetic field for various value along the cross-section of rod was found and plotted figure 3.8. The graph shows a very low cross-sectional variation of the axial magnetic field.

To determine the attainable isolation as a function of position in the axial magnetic field, F/B ratios were calculated

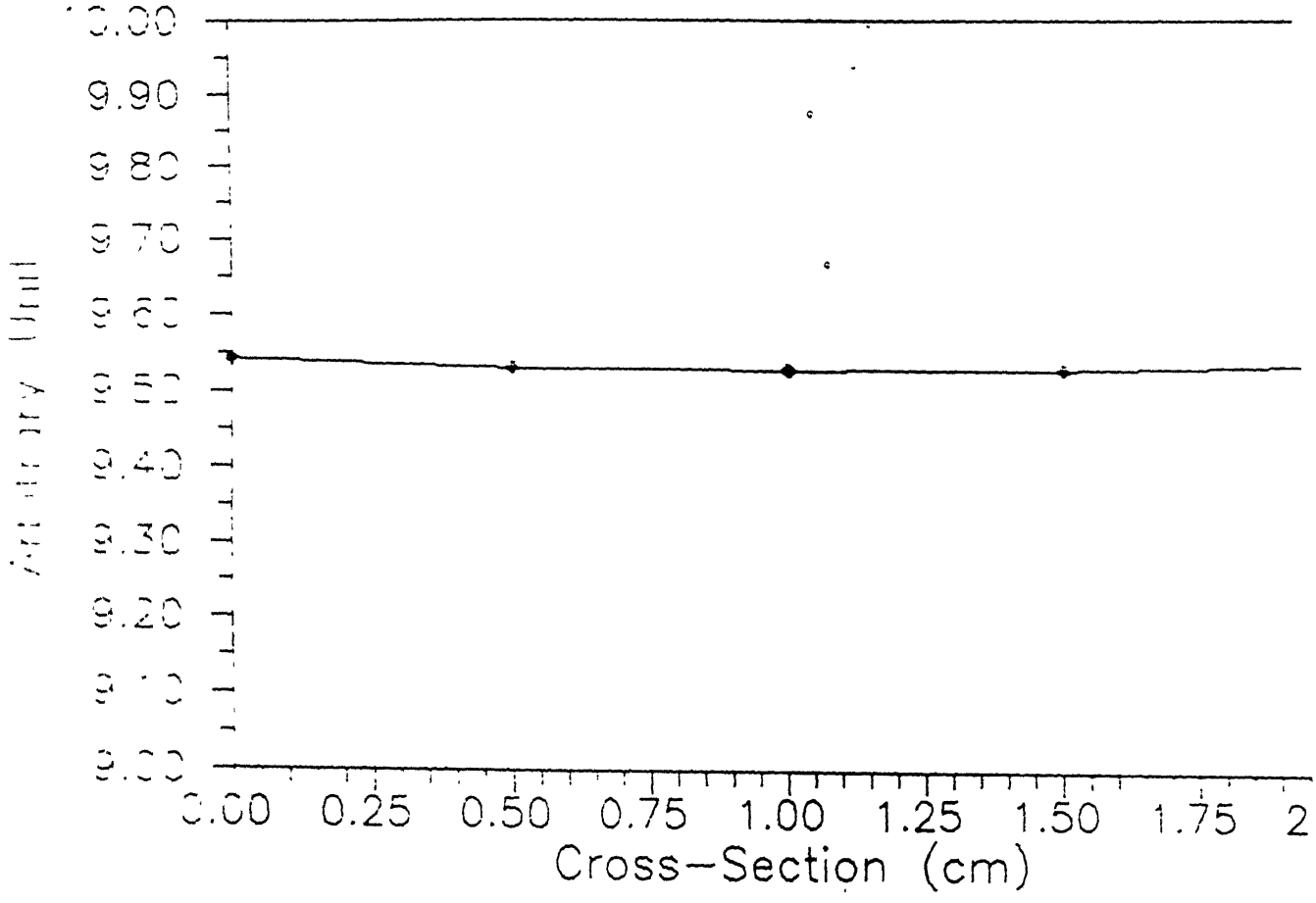

Fig.3.8 Cross–sectional variation of magneticfield

for four positions of the sample along the magnetic axis. The F/B ratios are given in the table 2 , where x is the distance from the outside edge of the solenoid to the rod end and $\Delta H/H$ is the effective magnetic field variation.

Table 2

x(cm)	F/B(dB)	$\Delta H/H = \pm 4/\pi(F/B)^{-1}$
2	20.8	0.010
2.7	25.7	0.0034
3.375	30.6	0.0011
4.25	38.1	0.0002

From the above table one can see that the effective magnetic field variation at the rod position is very low. To get very high F/B value,the magnetic field should be uniform over the whole cross-section.

Electronic circuit

To get the maximum magnetic field in the solenoid a capacitor bank is discharged through a spark gap circuit to provide enough current to energize the coil. The main part of the circuit is shown in the figure 3.9.This circuit can be assumed as an underdamped RLC series circuit. The current through the coil is given by[17],

$$i(t) = (V_0/\omega L)e^{-\alpha t}\sin\omega t \qquad \ldots\ldots(6)$$

where $\omega = [(1/LC)-(R/2L)^2]^{1/2}$; $\alpha = R/2L$ R-coil resistance

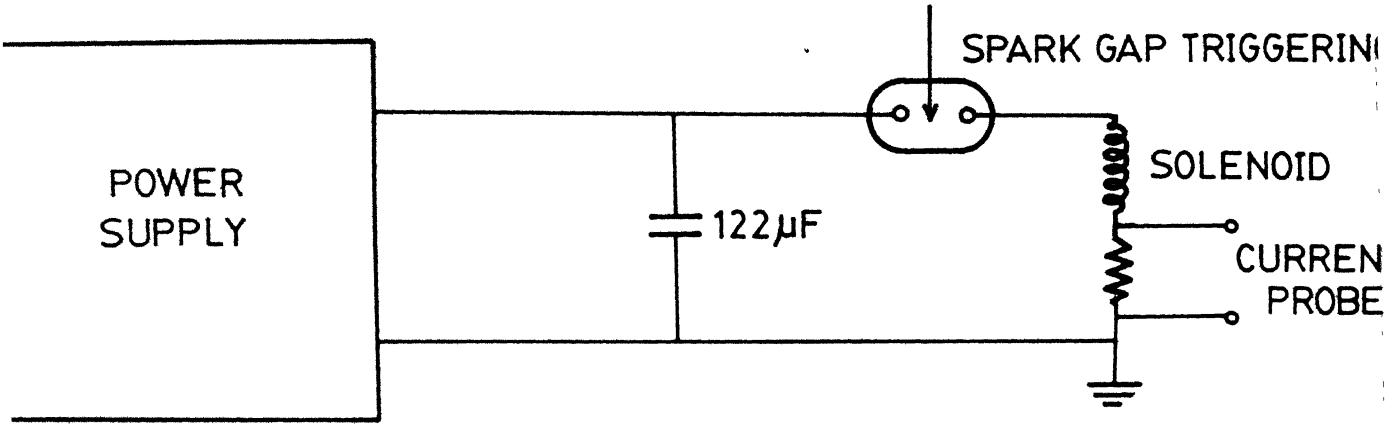

FARADAY ROTATOR SYSTEM.

IG. 3·9

L=coil inductance=$k\mu_o N^2 A/(4r^2+l^2)^{1/2}$ .....(7)

A=effective coil cross-sectional area.

The coil inductance was found to be 152μH using equation 7 .

The time required for the current to reach a peak is given by

$$t_p=(1/\omega)\tan(\omega/\alpha) \quad .....(8)$$

The circuit shown in the figure 3.9 has two parts.

i) charging unit ii) triggering unit

The charging unit contains a capacitor bank of value 122μF which can be charged from the power supply having a step up transformer and a voltage doubler. The required voltage to the capacitor bank can be calculated from equation (6) and is 925V. From equation (8) it follows that maximum time to reach the peak current is 0.108msec. The maximum current was found to be 730amp . Triggering can be done by using a triggering voltage circuit or with laser pulse triggering.

In conclusion the characteristics and performance characteristics of various components of Faraday isolator are reported. Unfortunately, due to non-availability of M-16 glass it was not possible to check the working characteristics of isolator.

CHAPTER 4

AIR BREAKDOWN NEAR SOLID TARGETS BY Nd:GLASS LASER

Introduction

Pirri[20] first observed low threshold optical breakdown of gases at the surface of a target using CO_2 lasers. The decrease in threshold laser energy was attributed either to thermal process or presence of metal plasma itself[21]. Breakdown of air at the surface of a metal using low power laser was reported by Bondarenko[22] and explained on the basis of thermal processes which accompany optical breakdown. It was observed that the presence of a precursor plasma[23] decreases the threshold intensity for breakdown of atomic and molecular gases. Short wavelength radiation emitted[24] from the metal plasma was also found to reduce the threshold intensity for breakdown of gases. Barchukov et al have proposed that an electron cascade can develope to ionize the gas surrounding the target due to metal vapour. We report air breakdown near solid targets (graphite,Al) using a free running Nd:Glass laser.

Experimental Setup

A free running Holobeam Nd:Glass laser, outlined in chapter 2 with output energy of upto 80 Joules and pulse width of 1-2msec and beam divergence of 4-5mrad was used for the experimental

studies. The laser beam was focussed by a lens of focal length 23.5cm (63cm) on to a solid target. To record the emitted spectrum, the plasma radiation was focussed on to a spectrograph. Simultaneously photographs of the plasma were taken with camera placed near to the target. The complete experimental setup is shown in figure 4.1.

Results and Discussion

Laser radiation was focussed on to a graphite target, placed in the atmosphere, using 23.5cm focal length lens. Intense visible plasma was observed with a characteristic cracking noise everytime laser hit the target. Spectrum was recorded using a three prisms spectrograph on the usual panachromatic photographic film. Every spectrum recorded is a collective effects of ten shots. The calibration was done by recording a mercury spectrum on the same film. The position of various spectrum lines were read using a comparator.

The spectrum lines were identified using spectrum line tables[25]. In addition to the standard spectrum lines of carbon, spectrum lines corresponding to nitrogen were also observed. The presence of these lines suggests that air is also breaking down. Table 3 gives the spectral lines observed with targets and those of carbon and nitrogen. The experiment was repeated with Aluminium as the target. Spectral lines were identified as above.

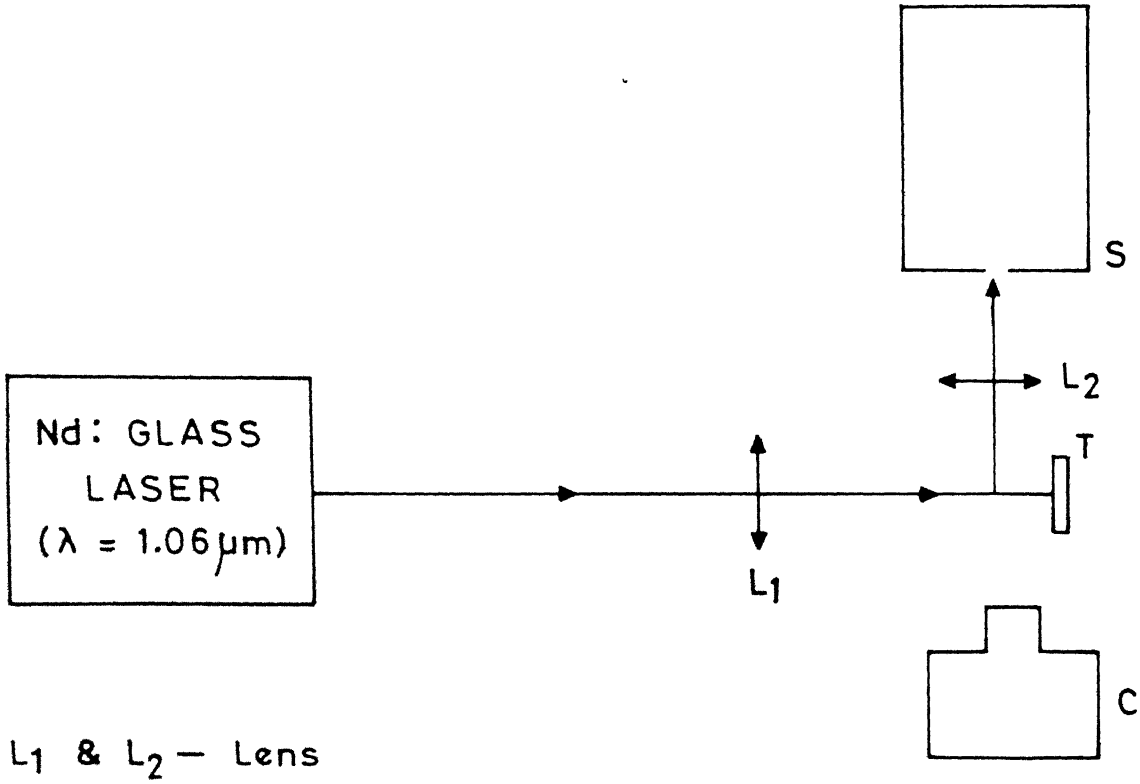

L_1 & L_2 — Lens

T — Target

S — Constant Deviation Spectrograph

C — Camera

Experimental Set-up for air Breakdown Studies in Presence of Metal Plasma.

FIG.4-1

Here again we observe characteristic lines corresponding for nitrogen. Since the resolution of our instruments is about 30A°, it is not possible to ascertain exact nature of breakdown. Air breakdown spectrum was recorded with Nd:YAG laser outlined in chapter 5. The air breakdown spectral lines are matching with the spectral lines observed as above.

The minimum intensity, I(W/cm^2), required for the development of an electron cascade in the gas is given by $I>6\times10^9 E_i/\lambda^2 A$ where E_i is the first ionization energy (ev) of the gas, λ the wavelength (μm) of laser radiation and A is the atomic (molecular) weight of the gas particle.

The condition of air breakdown is not satisfied in our case. The maximum laser intensity was found to be 2.23×10^6W/cm^2 for a pulse of energy 70 Joules, pulse width of 1msec and spot size of 1mm. This intensity is less than the threshold intensity (2.76×10^9W/cm^2) calculated from the breakdown condition. However if we account for the presence of the metal surface and we find that the condition is established for a period of the order of d/u where d is the spot size which is 1mm in our experiment and u is the speed of sound in vapour. This time was found to be 3×10^{-6}sec. In our experiment this time is very short compared to the laser pulse duration which is of the order of 1msec. In this time $d/u \ll \tau(10^{-6}\text{sec} \ll 1\text{msec})$ in the region of

dense vapour an electron cascade can develop due to the ionization of the air molecule by the vapour particles and as a result a spherical shock wave (point explosion) is produced in the air surrounding the target.

To get more evidence of breakdown of air in the presence of metal surface, the laser was focussed using lens with focal lengths 23.5cm and 63cm. It is observed that short focal length lens produces an intense spark but the extent of breakdown region is also small. On graphite target with focal length 23.5cm and laser energy 70J breakdown region as much as 10cm was observed. Small mean free path in the atmosphere increses the possibility of cascade ionization. Long focal length lens will have a long narrow beam waist and hence the possibility of increase in electron velocity and of collision is more which results in longer size of breakdown region. On decrease in laser energy decrease in extent of breakdown is observed. Figure 4.2 shows the variation of plasma size with input intensity in graphite target for focal length 23.5cm and 63cm.

In conclusion low threshold air breakdown in the presence of metal plasma was observed using the Nd:Glass laser outlined in chapter 2. Plasma length of as much as 10cm was observed by focusing laser radiation on graphite target. Decrease in plsma size was reported with input intensity.

Table 3 Spectral lines(A^{o})

Target: Al		Target: Graphite		Nitrogen	Air
Observed	Standard	Observed	Standard	Standard	Observed
6482	6698	6005	6688	6723	6907
6006	6696	5450	6683	6653	6439
5766	5557	5000	6674	6644	6077
5557	5107	4975	6671	6484	5202
5322	3961	4653	6663	6482	4775
4977	3944	4636	6662	6441	4296
4780	3935	4622	6655	6008	4219
4716	3931	4609	6654	5999	4177
4679	3482	4523	6653	5829	4157
4667	3479	4501	6587	5616	4138
4573	3458	4483	6397	5564	4132
4552	3452	4356	6016	5560	4108
4531	3444	4348	6014	5411	4103
4510	-	4340	6013	5356	4100
4489	-	4222	6012	4935	4068
4466	-	4212	6010	4914	-
4447	-	4195	6007	4494	-
4405	-	4181	6006	4492	-
4385	-	4171	6002	4358	-

4362	–	4155	6001	4336	–
4341	–	3992	5800	4317	–
4314	–	3960	5793	4305	–
4308	–	3911	5668	4223	–
4296	–	3902	5551	4151	–
4291	–	3875	5545	4137	–
4260	–	–	5380	4113	–
4231	–	–	5052	4109	–
4175	–	–	5039	4099	–
4048	–	–	5023	3830	–
4047	–	–	4932	3822	–
4033	–	–	4775	3650	–
–	–	–	4771	–	–
			4466		
			4371		
			4269		
			4228		
			4223		
			4212		
			4065		
			4029		
			4009		

ig.4.2 a) Variation of Plasma size with input energy in a graphite target.(Focal length of lens- 23.5cm)

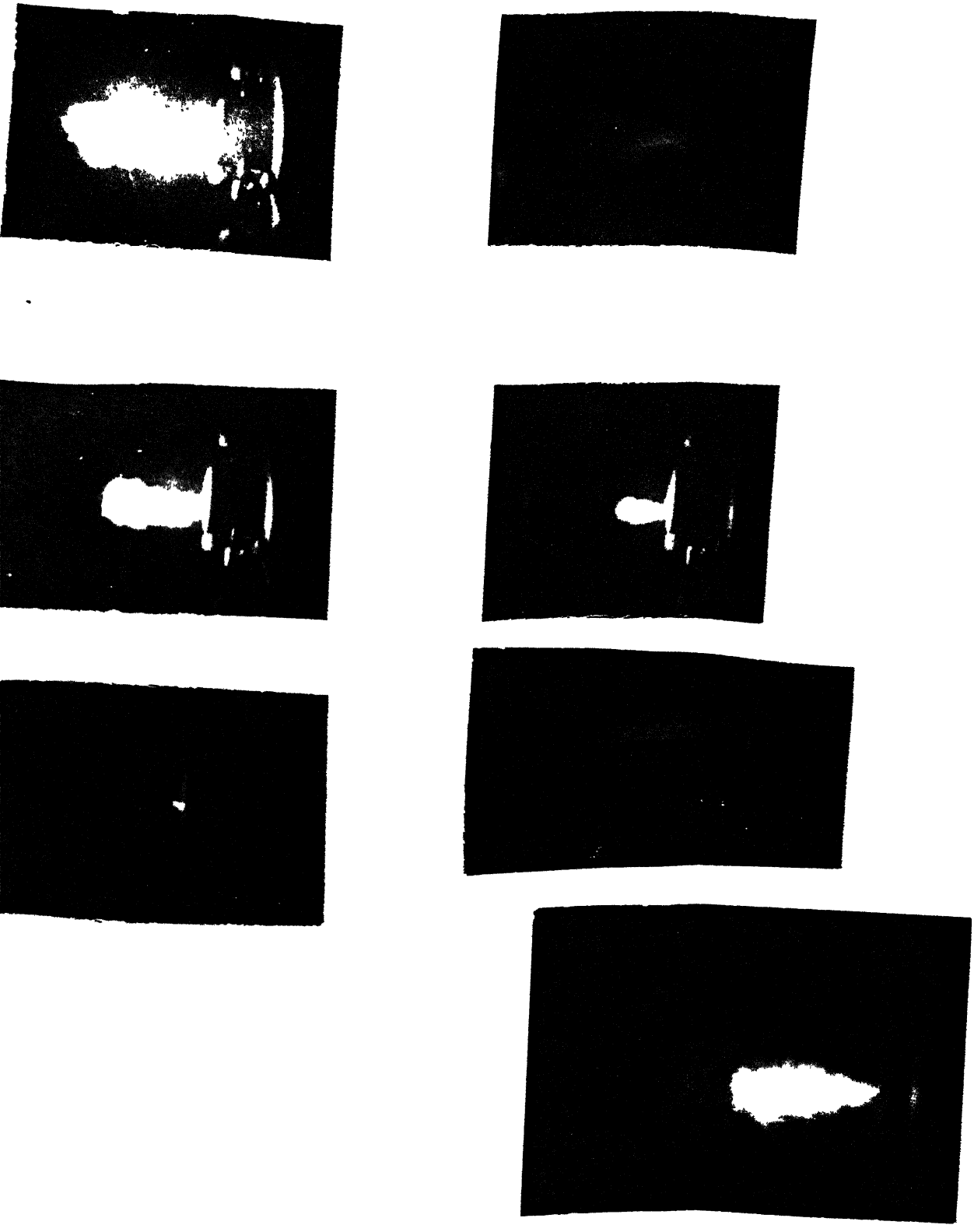

b) Variation of Plasma size with input energy in a graphite target.(Focal length of lens- 63cm)

CHAPTER 5

AIR BREAKDOWN USING YAG LASER AND ITS HARMONICS

Introduction

Since the first report of the laser induced breakdown of ai
in 1963, there has been an enormous growth of understanding o
the subject By focussing a laser beam in a gas it is possible t
get a high-temperature, high density plasma. The properties o
gaseous plasma created by focussing laser radiation have als
been studied. Laser produced plasmas have been used as source fo
high intensity X-rays and VUV continuum in rare gases
Sensitive techniques to measure UV radiation using gas breakdow
have also been developed. Lasers have been used to trigge
electrical discharge between electrodes in vacuum and in gases i
spark gap switches. Detailed calculations of the gas breakdow
threshold caused by laser irradiation have been carried out by
Kroll & Watson[26]. Buscher et al[27] were the first to study the
breakdown threshold intensity of rare gases at wavelengths
1.06, 0.69, 0.53 and 0.35μm. They found that the threshold
intensity for each rare gas studied first increases to a
maximumandthen decreases with decreasing wavelength. Alcoc
al[28] reported the breakdown ofnitrogen, methane and rare g
using a ruby laser of pulse width 20ns and its second harmc

in agreement with Buscher et al and Krasyuk et al[29] studied the breakdown threshold of nitrogen, helium and argon using ps pulses of ruby laser in the pressure range $2 \leq p \leq 10^4$ torr. The results show a weak dependence on the pressure for $p \leq 10^3$ torr in He and Ar and $p \leq 300$ torr in N_2, characteristic of multiphoton absorption. At higher pressure in He and Ar there is a pronounced p dependence, indicating the occurance of collisional ionization by inverse bremsstrahlung absorption, however for N_2 the p dependence is less pronounced. Gamal et al[30] and Weyl et al[31] have done theoretical calculations of laser induced breakdown thresholds of atomic and molecular gases as a function of pressure of the gas, pulse width of laser using the equation of growth of electrons, and including the effects of both MPI and cascade ionozation. In this thesis, we report the preliminary studies on air breakdown by focussing the Nd:Yag laser and its harmonics at various pressures, in the range of 24-760 torr. Dependence of the size of visual spark as a function of laser radiation is also studied.

Experimental setup

A schematic of the experimental set up used is shown in figure 5.1. A Nd:Yag laser (DCR-4, spectra physics) and its harmonics delivering upto 900 mJ in 2.5 ns in fundamental with a repitition rate of 10pps, was focussed with a quartz lens

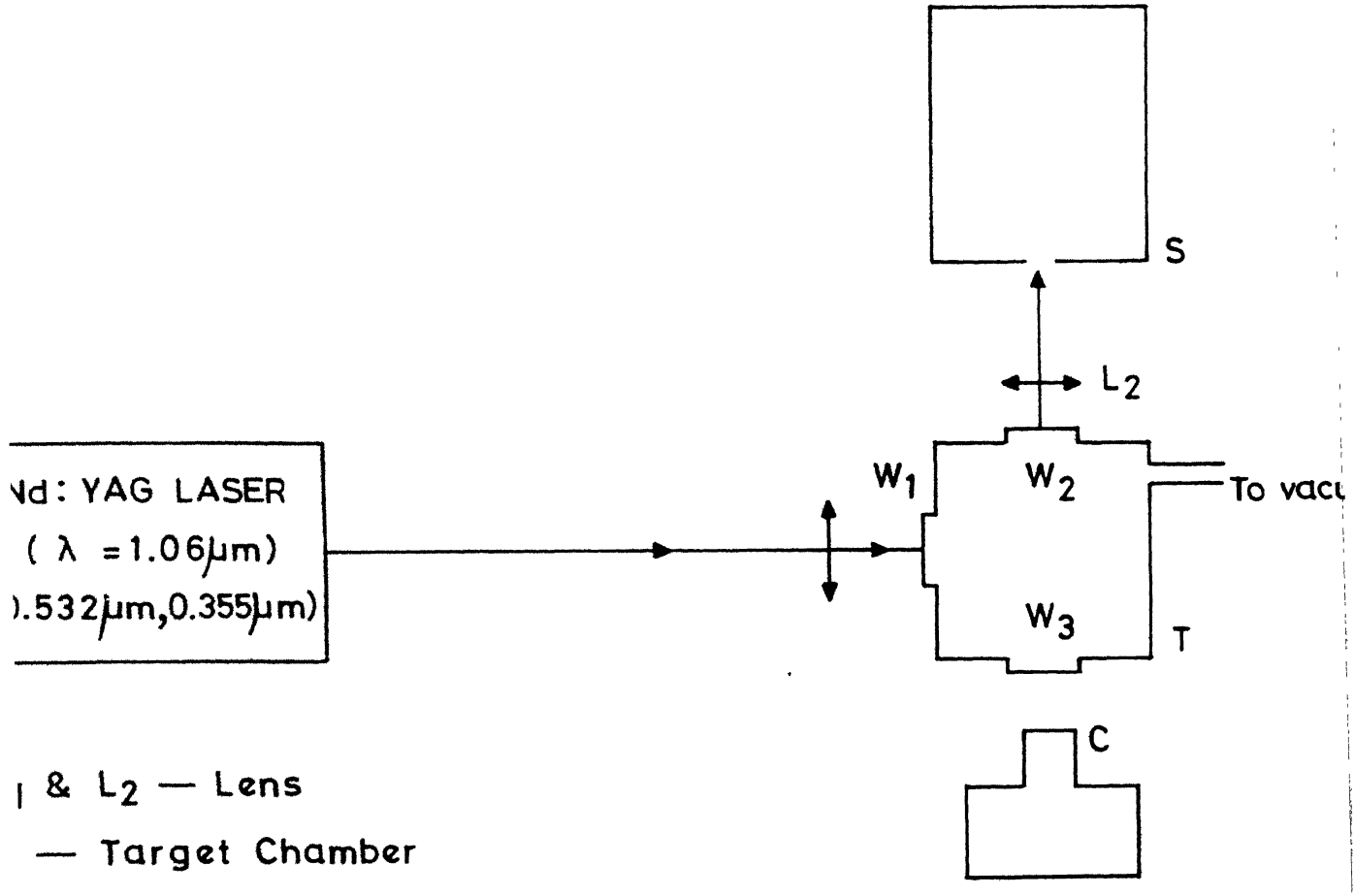

1 & L_2 — Lens

— Target Chamber

1 W_2 & W_3 — Quartz Windows

— Constant Deviation Spectrograph

— Camera

xperimental Set-up for Air-breakdown Studies.

FIG. 5.1

(f=12cm) in the centre of a vaccum chamber. The chamber was evacuated to $<10^{-2}$torr with a rotary pump. Laser energy was varied by reducing the firing voltage of the laser (always above threshold voltage). The energy of the laser was measured with a laser power meter (Ophir), by placing the power meter in the path of the main beam. Threshold energy was measured only when the breakdown spark seen visually through the window, was modulated at 10pps. Breakdown spot size was recorded using a camera.

Results and Discussion

Figure 5.2 shows the dependence of breakdown threshold intensity on wavelength of laser radiation used for different pressure of air. This shows that threshold intensity first increases to a peak and then decreases with increasing wavelength at a pressure of 390 torr. At longer wavelengths the irradiance required for gas breakdown decreases with increasing wavelength, in accordance with cascade collision ionization theory. On the other hand, at visible wavelength, the irradiance threshold required to breakdown at low or moderate pressure of air decreases with decresing wavelength because of photoionization of excited atoms and resonant absorption effects. These results are in agreement with Buscher etal. However at atmospheric pressure of air it is observed that the threshold intensity first decreases to a minimum and then increases with incresing

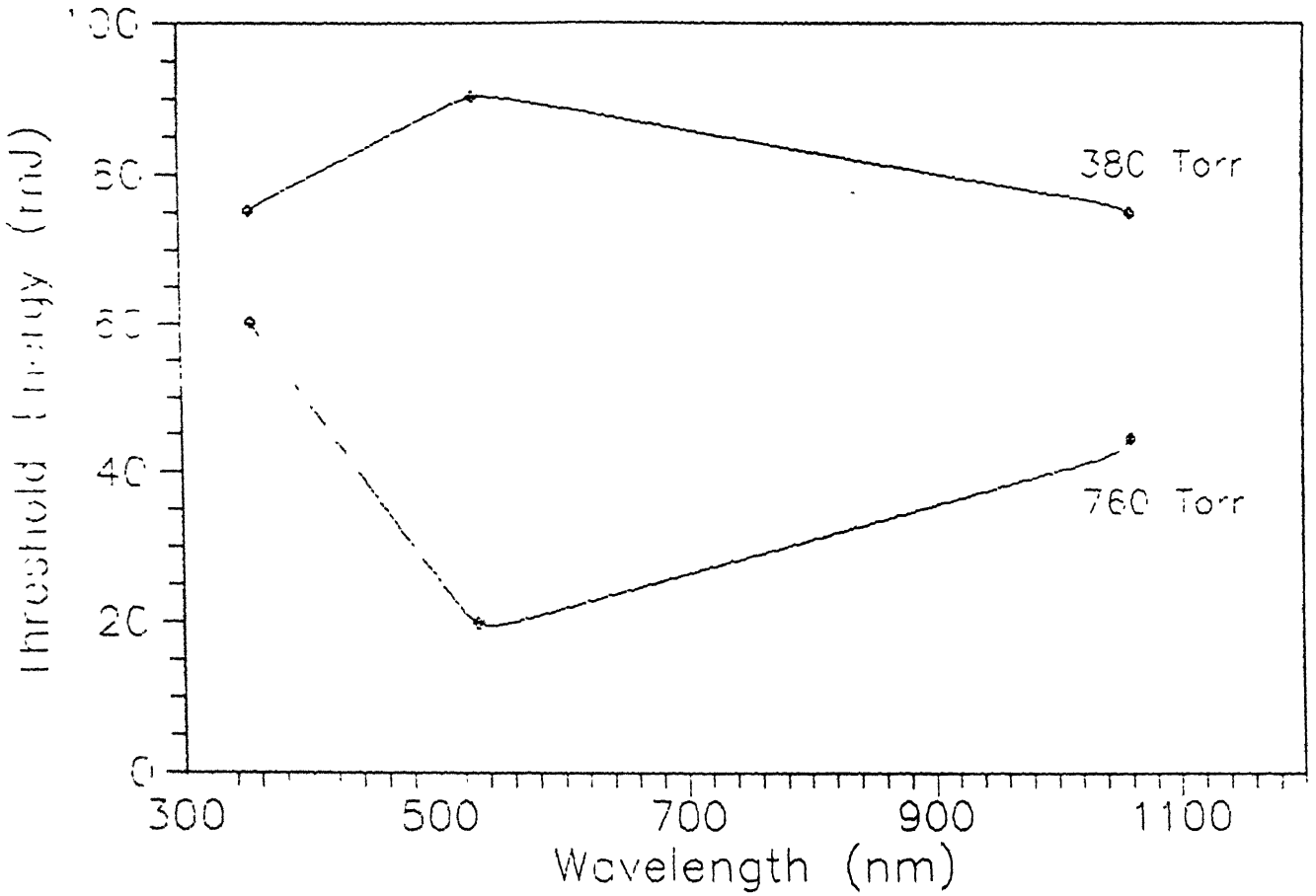

Fig. 5.2 Wavelength dependence of Threshold Energy

wavelength in contradiction to Buscher's result. Breakdown threshold intensity was measured for atmospheric air inside and outside the chamber. It is also observed that threshold intensity is less outside the chamber as compared to inside the chamber. It is expected since breakdown threshold intensity can be reduced as compared to the case of still air.

Figure 5.3 shows the dependence of threshold intensity on pressure of air for different laser wavelengths. It is observed that threshold intensity increases with the decrease of pressure. At low pressures the collision frequency is low, sufficient ionization can be maintained by increasing the probability of ionization at each collision (consequently the electron velocity) and thus electric field associated with laser radiation should be high. Hence threshold intensity increases as pressure decreases. Breakdown threshold intensity of air at 1.06μm shows pronounced p dependence, characteristic of collisional ionization by inverse bremsstrahlung absorption, however weak dependence is observed for 0.532μm and 0.355μm laser irradiation, indicating the occurrence of miltiphoton absorption. Thus the breakdown of air may be initiated with multiphoton absorption and then proceed due to cascade process.

Figure 5.4 shows the variation of length of visible spark with 1.06μm laser energy radiation at atmospheric pressure. It is

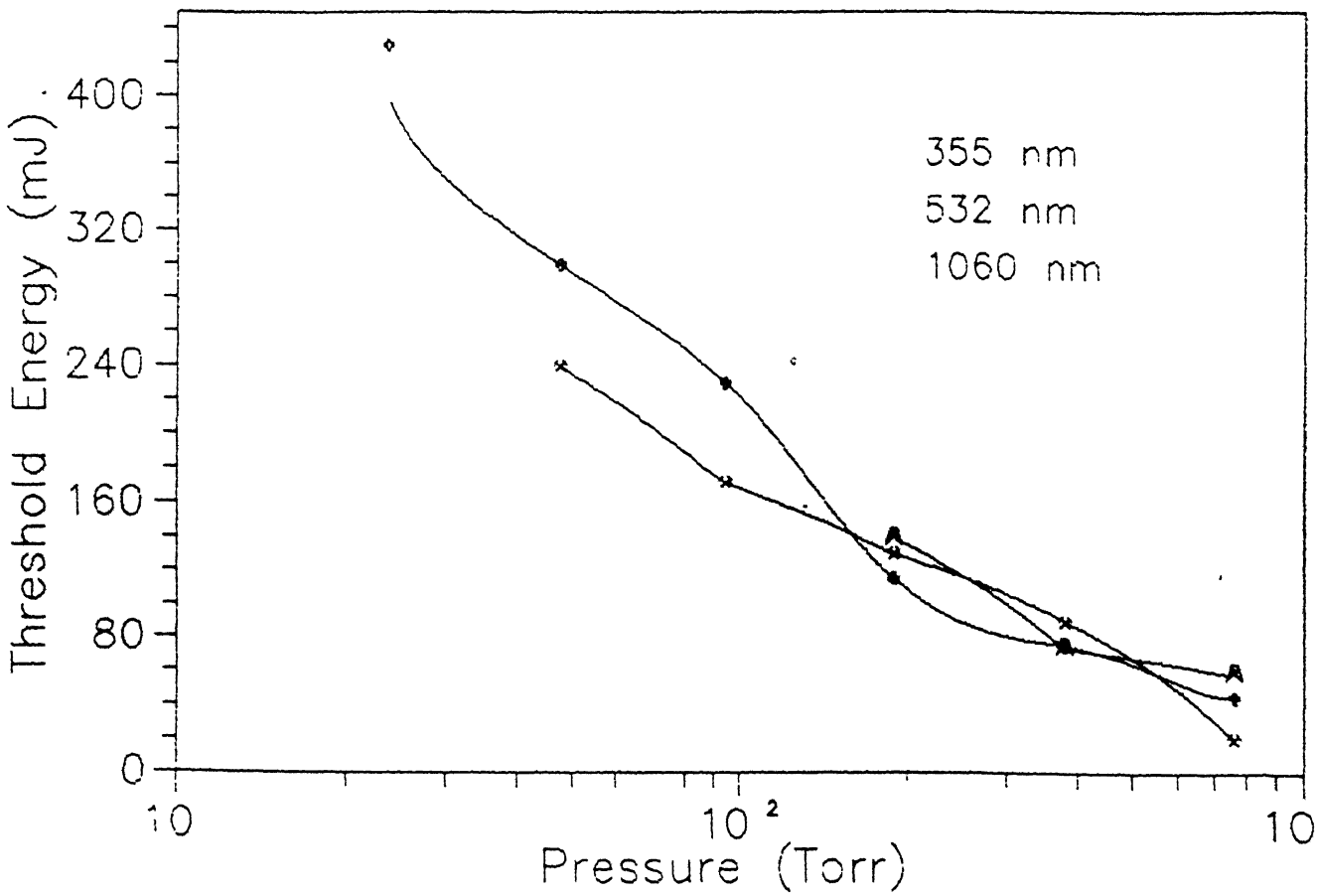

Fig. 5-3 Pressure dependence of Threshold Energy

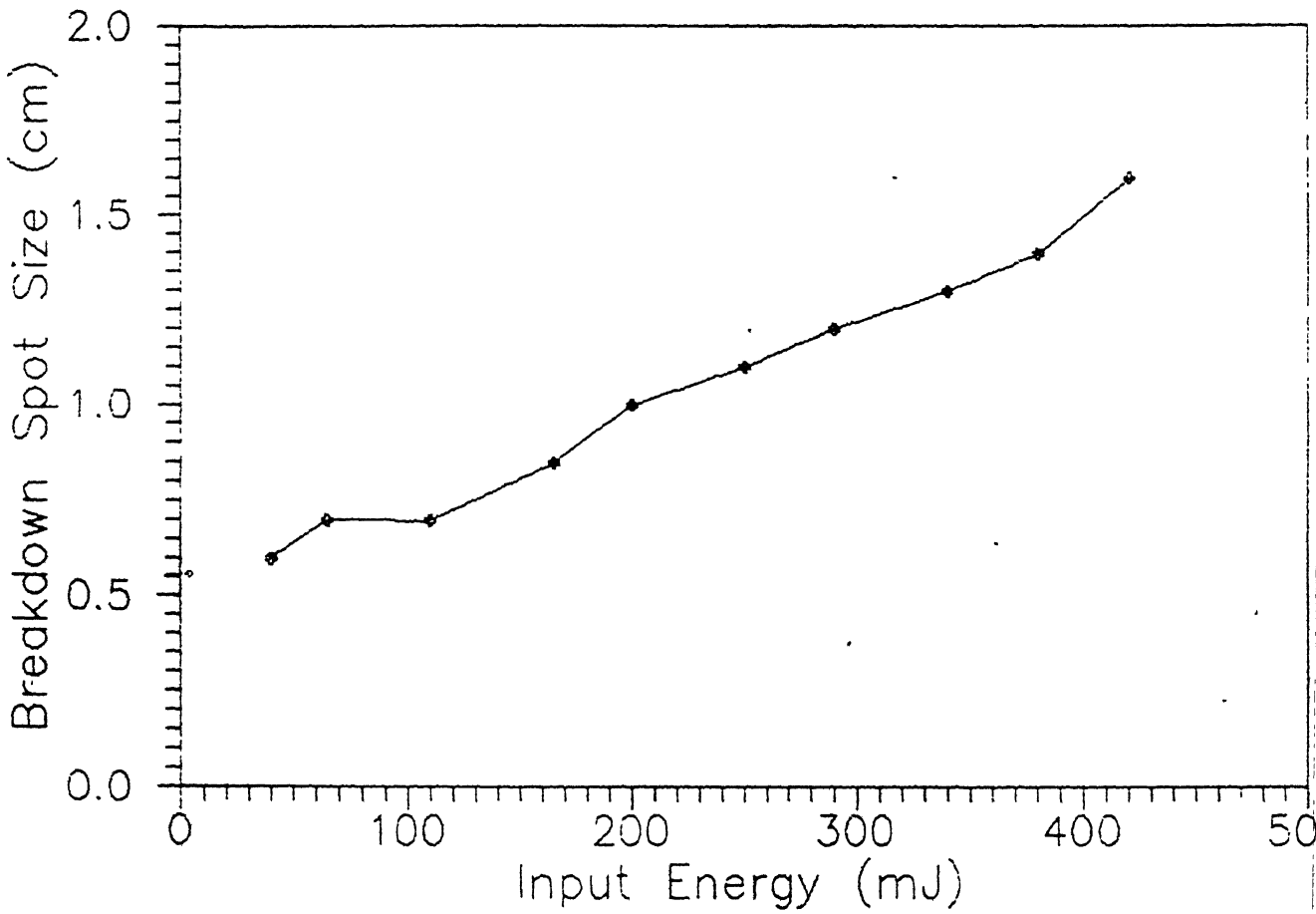

Fig.5.4 Breakdown Spot Size variation with Input Energy

observed that length of the visible spark increases with the increase of laser energy. As the energy contained in the beam waist, increases, length of visible spark increses. No appreciable change of spot size (length or width) was observed with the pressure of air with 1.06μm radiation.

In conclusion, air breakdown was observed visually with Nd:Yag laser and its harmonics at various pressures, in the range of 24-760 torr. Breakdown threshold intensity was found to be dependent on wavelength and pressure. Breakdown spot size is strongly dependent on the laser radiation and weakly dependent on the pressure of air.

CHAPTER 6

CONCLUSIONS

An existing Nd:Glass is upgraded to give energy of 80J per pulse in free running mode. By focussing laser on to a solid target we investigated the breakdown characteristics of air near the solid target. No breakdown of air was observed by focussing laser radiation without the metal surface irrespective of the focal length of the focussing lens. The extent of the breakdown region near the metal surface depends on the focal length of the focussing lens and the focussed spot on the target. The results are reported for breakdown of air using graphite and aluminium target. To avoid the back reflected laser radiation from the laser produced plasma into the laser cavity, a Faraday isolator was designed. The characteristics of various components designed for Faraday isolator are presented. Preliminary results on the laser induced breakdown of air using Nd:YAG laser and its $2w_o$, $3w_o$, $4w_o$ are reported. The wavelength and pressure dependence of breakdown threshold was studied and presented in this report. The variation of breakdown spot size with energy also studied.

The results reported in this are preliminary investigations. To get more information on the effect of target on breakdown of air, a systematic study using different target material shall be done. Similarly, breakdown studies without the metal surface are

to be performed at still lower pressure, to ascertain the pressure dependence.

Faraday isolator has been designed, but the working of it will become clear only when M-16 rod is available.

References

1. P.D. Maker et al, Procedings of the 3rd International conference on Quantum Electronics, edited by P.Grivet, and N Blombergen (Columbia, New york 1963), pp.1559-1565.

2 R.G. Mayerand et al, Phys.Rev.Lett.11,401(1963).

3 Agostini et al, IEEE J.Quant.Electron QE-6,782(1970).

4 Gray Morgon, Rep.Prog.Phys. 38,621(1975).

5. A.H. Guenther et al J.Phys.D:Appl.Phys.11,1577(1978).

6. V.A. Batanov et al, Sov.Phys.JETP 50(6),1979.

7. David C. Smith, J.Appl.Phys. 41,4501(1970).

8. A.M. Robinson, Appl.Phys.Lett. 22,33(1973).

9. A.A. Vedenov et al Sov.J.Quant.Electron 11,896(1981).

10. A.I. Barchukov et al, Sov.Phys.JETP 39,469(1974).

11. Yu.P. Raizer, Laser-induced Discharge Phenomena (Consultants Bureau, New York,1977) Chapter 1.

12. Bebb & Gold, Phys.Rev. 143,1(1966).

13. W.Kochner, Solid-state Laser Engineering, Springer Series in Optical Sciences 1976.

14. Jenkins & White, Fundementals of optics, New York McGraw Hill, 1957.

15. K. Eidmann et al, Journal of Physics E: Sci.Inst,5,56(1972).

16. George R. Bird, JOSA vol49,235(1959).

17. Fong, The Rev.Sci.Inst. vol.41,1434(1970).

18. Padula et al, IEEE J Quantum Electronics, QE-3,493(1967)

19. D.B. Montgomery, Solenoid Magnetic Design, Wiley-Interscience,1969, Chapter 8.

20. Pirri et al, Appl.Phys.Lett.21,79(1972).

21. M.G. Drouet, Appl.Phys.Lett. 31,647,(1977).

22. Bondarenko et al, Sov.Phys.Dokl, 25,616,(1980).

23. Dan'shchikov et al, Sov.J.Quant.Electron.12,62(1982).

24. J.M. Green J.Appl.Phys. 48,2753(1977).

25. A.N. Zaidel, Tables of Spectrum lines, 1961.

26. Kroll & Watson , Phys. Rev. 45, 1883(1972).

27. Buscher et al, Phys. Rev.Lett.15, 847(1965).

28. Alcock et al, Opt.Commun. 6, 342(1972).

29. P.N. Krasyuk et al, Sov. Phys.JETP 31,860(1970).

30. Gamal et al, J. Phys.D: Appl. Phys. 14, 2209(1971).

31. Weyl et al Phys. Rev.A31, 2300(1985).

LTP-1990-M-MUT- UPG